Ministry of Higher Education and Scientific Research

وزارة التعليم العالي والبحث العلمي

Badji Mokhtar Annaba University
Université Badji Mokhtar Annaba
Faculty Of Technology
Electromechanics department

جامعة باجي مختار – عنابـــــــــة
كلية التكنولوجيا
قســـــــم الالكتروميكانيك

Thesis

Presented in view of obtaining the diploma of

Doctorate

Speciality: Electromechanics
Field: Electromechanics

By
Maroua MEKCEM

Master in energetics and environment

Theme

Contribution to the improvement of heat transfers in heat pipes using nanofluids

Thesis defended ahead the jury composed of:

Pr. Elias HADJADJ AOUL	Badji Mokhtar University- Annaba	President
Pr. Hocine CHEGHIB	Badji Mokhtar University- Annaba	Reporter
Dr. Muhittin BILGILI	Gazi University- Ankara	Co- Reporter
Pr. Hocine MZAD	Badji Mokhtar University- Annaba	Examiner
Dr. Samah ADJMI	Université Chadli Benjedid- El Taref	Examiner
Pr. Mohamed KHEZZAR	20 Aout 1955 University- Skikda	Examiner

2024/2025

Acknowledgments

First and foremost, I want to give thanks and praise to Allah, the Almighty, who has given me many opportunities, blessings, and knowledge, enabling me to finally complete the thesis. For me, pursuing this PhD has been a genuinely transformative experience, and I could not have done it without help of Allah.

With great sadness and sorrow, I would like to pay my gratitude and my respects to the deceased ***Dr Mahieddine BERKANI****, who was an Associate Professor at the University of Badji Mokhtar Annaba, Algeria. He supervised me throughout this thesis, he was kind, and he encouraged me all the time. May God have mercy on him.*

I would like to thank ***Pr Hocine CHEGHIB*** *Professor at the University of Badji Mokhtar Annaba, Algeria, who supervised me and continued with me the doctoral path. I would like to thank him for his kindness, and for the numerous encouragements he gave me.*

I would like to thank ***Dr Muhittin BILGILI****, Associate Professor at Gazi University Ankara, Turkey, who co-supervised me throughout this thesis. I would like to thank him for his kindness, and for the numerous encouragements he gave me.*

I would like to thank the president of the jury, ***Pr Elias HADJADJ AOUL****, A Professor at the University of Badji Mokhtar Annaba who kindly did me the honour of presiding over this jury. My thanks also go to* ***Pr.Hocine MZAD****,* ***Dr.Samah ADJMI*** *and* ***Pr. Mohamed KHEZZAR*** *for the honor of being my thesis jury members.*

Last but not least, I thank my Family and my Parents, without whom I would not be here.

Special thanks to my dear husband who has always been supportive and helped me to get through this path and its difficult moments, without forgetting our son, my little baby who made this experience special and brilliant, because I wrote these words while holding him into my arms.

Abstract

Heat pipes are highly effective heat transfer devices used for thermal management in different fields. The working fluid within the heat pipes provides the heat transport from the evaporator to the condenser and limits their thermal performance. Thus, substitution of conventional working fluids with nanofluids has been a promising solution to enhance the thermal performances of heat pipes.

The wickless gravity assisted heat pipe, called also Two-phase closed thermosyphon (TPCT) is the subject of this study, regarding its importance in various applications such as, permafrost de-icing, solar collectors, nuclear reactors and heat recovery systems.

This study provides important findings of an experimental investigation performed on a miniature copper two-phase closed thermosyphon using three different cellulose nanofiber concentrations with three filling ratios at different heat loads. Effects of these parameters on wall temperature, thermal resistance, and startup are analysed and compared to each other. Furthermore, transient wall temperature variation from the minimum to the maximum applied heat load is analysed for cases of highest and lowest wall temperature distribution.

Keywords: Heat pipes; Two-phase closed thermosyphon; nanofluid; cellulose nanofiber; Filling ratio; Thermal efficiency.

Résumé

Les caloducs sont des dispositifs de transfert de chaleur très efficaces, utilisés pour la gestion thermique dans différents domaines. Le fluide de travail à l'intérieur des caloducs assure le transport de la chaleur de l'évaporateur vers le condenseur et limite ses performances thermiques. Ainsi, la substitution des fluides de travail conventionnels par des nano fluides s'est avérée une solution prometteuse pour améliorer les performances thermiques des caloducs.

Le caloduc sans mèche assisté par gravité, également appelé thermosiphon fermé biphasé (TPCT), fait l'objet de cette étude, compte tenu de son importance dans diverses applications telles que le dégivrage du pergélisol, les capteurs solaires, les réacteurs nucléaires et les systèmes de récupération de chaleur.

Cette étude fournit les résultats importants d'une étude expérimentale réalisée sur un thermosiphon fermé biphasé miniature en cuivre utilisant trois concentrations différentes de nanofibre de cellulose avec trois taux de remplissage à différentes charges thermiques. Les effets de ces paramètres sur la température des parois, la résistance thermique et le démarrage sont analysés et comparés les uns aux autres. En outre, la variation transitoire de la température des parois depuis la charge thermique appliquée de sa valeur minimale jusqu'au maximale est analysée pour les cas de distribution de température de paroi la plus élevée et la plus basse.

Mots-clés : Caloducs ; Thermosiphon fermé biphasé ; nanofluide ; nanofibre de cellulose ; Taux de remplissage ; Efficacité thermique.

ملخص

تعتبر الأنابيب الحرارية أجهزة فعالة للغاية لنقل الحرارة وتستخدم لإدارة الحرارة في مجالات مختلفة. يوفر سائل العمل داخل الأنابيب الحرارية نقل الحرارة من المبخر إلى المكثف ويحد من أدائه الحراري. وبالتالي، كان استبدال سوائل العمل التقليدية بالسوائل النانوية حلاً واعداً لتعزيز الأداء الحراري لأنابيب الحرارة.

إن الأنابيب الحرارية المدعومة بالجاذبية عديمة الفتيلة، والتي تسمى أيضًا السيفون الحراري المغلق ثنائي الطور، هي موضوع هذه الدراسة، نظرًا لأهميتها في تطبيقات مختلفة مثل إزالة الجليد من التربة الصقيعية، ومجمعات الطاقة الشمسية، والمفاعلات النووية، وأنظمة استعادة الحرارة.

تقدم هذه الدراسة نتائج مهمة للبحث التجريبي الذي تم إجراؤه على سيفون حراري مغلق ثنائي الطور من النحاس باستخدام ثلاثة تراكيز مختلفة من ألياف السليلوز النانوية مع ثلاث نسب تعبئة عند أحمال حرارية مختلفة. يتم تحليل تأثيرات هذه المعلمات على درجة حرارة الجدار والمقاومة الحرارية وبدء التشغيل ومقارنتها ببعضها البعض. علاوة على ذلك، تم تحليل اختلاف درجة حرارة الجدار العابر من الحد الأدنى إلى الحد الأقصى للحمل الحراري المطبق في حالات توزيع درجة حرارة الجدار الأعلى والأدنى.

الكلمات المفتاحية: مواسير حرارية; سيفون حراري مغلق ثنائي الطور؛ السائل النانوي؛ ألياف السليلوز النانوية؛ نسبة الملء الكفاءة الحرارية.

Scientific Production

Publication in international journals

Mekcem, M., Berkani, M., & Bilgili, M. (2024). Impact of filling ratio and cellulose nanofiber nanofluid on the total thermal resistance and the startup of a miniature thermosyphon. Heat Transfer Research, 55(17), 1–12. doi: 10.1615/HeatTransRes.2024051883

Publication in international conferences

Mekcem, M. (2018). Nanofluids and heat pipe limitations. Academic Perspective Procedia, 1(1), 298–304. doi: 10.33793/acperpro.01.01.58

Table of Contents

CHAPTER II: State of The Art on Two-phase closed thermosyphons Using Nanofluids

CHAPTER III: Heat Transfer Enhancement in TPCT Using Cellulose Nanofiber: Experimental Study

CHAPTER IV: Results and Discussion

List of figures

CHAPTER I: Overview On Heat Pipes And Nanofluids

CHAPTER II: State Of The Art On Thermosyphons Using Nanofluids

CHAPTER III: Heat Transfer Enhancement in TPCT Using Cellulose Nanofiber: Experimental Study

CHAPTER IV: Results and Discussion

List of tables

CHAPTER I: Overview On Heat Pipes And Nanofluids

CHAPTER III: Heat Transfer Enhancement in TPCT Using Cellulose Nanofiber: Experimental Study

Nomenclature

Acronyms

TPCT: two-phase closed thermosyphon

FR: Filling ratio

DI: Deionized water

CNF : Cellulose Nanofiber

BHTC: Boiling heat transfer coefficient (W/m^2K)

CHTC: Condensation heat transfer coefficient (W/m^2K)

Notation

η: Efficiency (%)

R_{tot} : Total thermal resistance (K/W)

T: Temperature (K)

A: Surface (m^2)

D: Diameter (m)

L_c : Characteristic length (m)

k: Thermal conductivity (W/m.K)

h: Heat transfer coefficient (W/m^2K)

Nu : Nusselt number

Pr : Prandtl number

Re : Reynolds number

V: Air flow velocity (m/s)

ρ: Density (kg/m^3)

μ: Dynamic viscosity (kg/m.s)

Cp: Specific heat (J/kg)

Φ **:** volume concentration (vol.%)

Subscripts

nf: Nanofluid

bf: Base fluid

n: Nanoparticles

e: Evaporator

c: Condenser

i: Inner

o: Outer

v: Vapor

f: Film

∞ : Ambient

General Introduction

Heat pipes are efficient thermal management devices, employed in various applications, such as: electronic cooling, HVAC systems, solar systems, fuel cells cooling, permafrost stabilization, heat waste recovery systems, satellite thermal control, nuclear reactors, medicine and human body temperature control.

Due to their reliability, compact and robust design heat pipes gained a resounding interest in the last decades. In nowadays, as the need of thermal control rises, enhancing heat transfer within heat pipes became a necessity. The heat transfer improvement can decrease the energy loss and scale down the heat pipe size. Therefore, scientists have been striving to optimize the operation conditions. Since, heat pipes work with the latent heat of working fluid, improving its thermophysical properties was a great idea to enhance heat transfer rate without using external energy or enlarging the heat exchange surfaces. Thus, substitution of conventional working fluids with nanofluids was found to be an alternative that improve the efficiency of heat pipes. Several experimental and numerical studies have shown that nanofluids improved heat transfer in heat pipes to some limits. Yet, high cost of nanofluids production and sedimentation of nanoparticles within still represent a standing challenges.

This study aims to contribute to heat transfer improvement of a Two-phase closed thermosyphon by using a nanofluid based on the ecofriendly cellulose nanofiber, which is non-frequently used.

Thesis is structured as follow: The first chapter provides an overview on heat pipes and nanofluids, allowing the redear to recognize the domain of heat pipes and nanofluids. Furthermore, impacts of nanofluids on heat pipes thermal performance are summarized. Whereas the second chapter possesses the state of the art on Two-phases closed thermosyphons using nanofluids. The third chapter represents the experimental study performed to investigate the contribution of cellulose nanofiber and filling ratio in heat transfer enhancement in a miniature two-phase closed thermosyphon. Results are discussed in the fourth chapter, followed by a general conclusion and perspectives for future studies.

CHAPTER I

Overview On Heat Pipes And Nanofluids

I.1. Introduction :

Du to their efficiency and reliability, heat pipes have been gaining a resounding interest in the last decades. Heat pipes are heat transfer devices implemented in various engineering domains, such as, electronic cooling, solar systems, fuel cells cooling, permafrost stabilization, aerospace thermal control, nuclear reactors, medicine and human body temperature control. This chapter represents a study of the art on heat pipes, including their history, operation principle, different main types and designs of heat pipes. Furthermore, adoption of nanotechnology and specifically nanofluids to enhance their thermal performance is discussed. This given general perspective helps to recognize heat pipes and their importance in thermal management.

I.2. Brief history of the heat pipe :

The predecessor of the heat pipe is the Perkins tube, which was invented by the American Angier March Perkins in the mid-19th century in UK, then it was developed by Perkins family through a series of patents till the 20th century.

The first closest heat pipe design to nowadays heat pipe was conceived by Gaugler in 1944 for General Motors Corporation in the U.S, but his idea recessed and was not used for a refrigeration problem. Serious development started in 1964 when Grover filed a patent application by reinvention of the heat pipe at Los Alamos National Laboratory in New Mexico. Grover and his co-workers demonstrated the reliability of heat pipes as an effective heat transfer device and proposed various application domains. The heat pipe knew a scientific renewal since 1985. This successive development was motivated to overcome the need to resolve different cooling issues in different fields.[1,2].

I.3. Operation principle of heat pipe:

In base, the heat pipe is a hollow sealed metal tube evacuated of air and filled with a small amount of a vaporizable liquid called working fluid. This filling amount is set to a filling ratio which is the volume of the working fluid to the evaporator section volume. Manly, the heat pipe is divided into three sections: evaporator, condenser and adiabatic section. The heat applied to the evaporator section vaporizes the working fluid, and then the vapor spreads in the adiabatic

section toward the condenser where it condenses and provide the heat sink releasing its latent heat of vaporization. Thereafter, the condensate returns back to evaporator section by a driving force and by this process the heat pipe works passively and continuously. The driving force used to return the liquid from the condenser to the evaporator differs according to the type of heat pipe. It could be gravitational, capillary, centrifugal, electrostatic and osmotic force [3].

I.3.1. Types of heat pipes :

All heat pipes work with same principle of phase change. It exists different heat pipe types classified according to their construction, geometry and type of the dominant driving force. The most distinguished heat pipes are defined below, noting that it exists also other subcategories and nonconventional heat pipes shapes (Bent, flattened, twisted...etc), even a heat pipe may have multiple evaporators, condensers and adiabatic sections. This variety of design allowed the heat pipe widely used in various thermal management technologies.

I.3.1.1. Conventional heat pipe:

The conventional heat pipe is a closed tube which could be flattened or bent, containing a porous structure called wick or mesh tacked on its inner surface. Fig I.1. The condensate can move against the gravity thanks to the capillary force ensured by the pores of this structure, and that why the conventional heat pipes are widely used in electronic devices cooling and aerospace crafts. Typical wick designs are mentioned in Fig I.2.

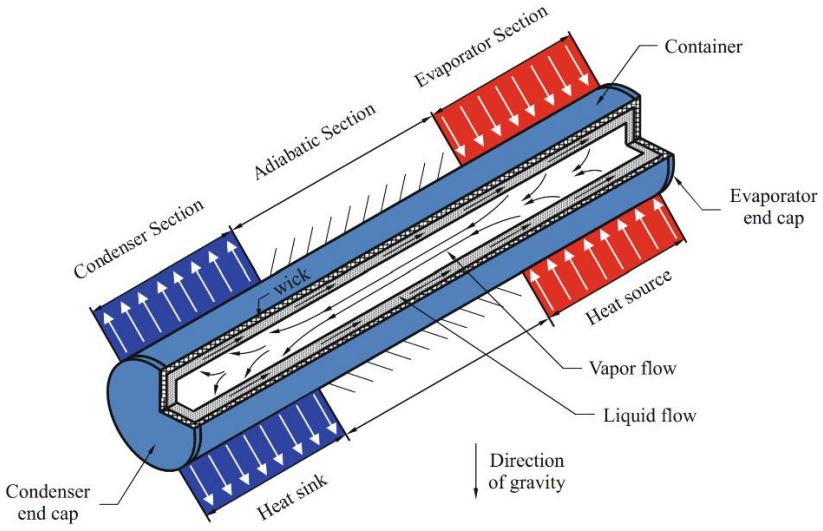

Fig I.1: Conventional heat pipe [4]

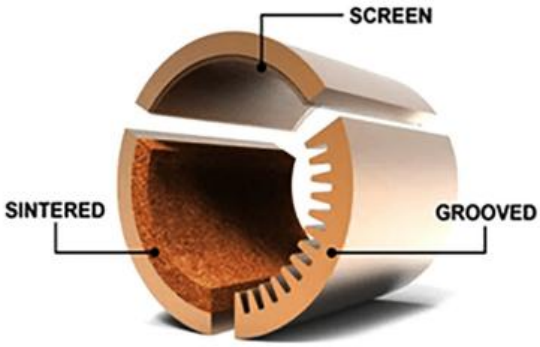

Fig I.2: Typical wick designs [5]

I.3.1.2. Two-phase closed thermosyphon (TPCT):

Is a wickless gravity assisted heat pipe with a simple design, in which the condenser is located above the evaporator which ensure the return of condensate by gravitational force. Fig.3. The TPCT is applied in heat waste recovery systems, solar collectors, geothermal systems and other cooling systems.

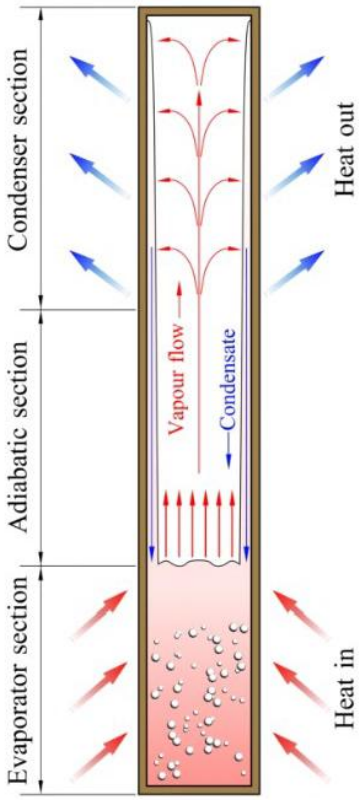

Fig I.3: Wickless gravity assisted heat pipe or Thermosyphon [6]

I.3.1.3. Rotating Heat Pipe (RHP):

Is a wickless heat pipe consisting of a rotation axe. Rotation about the axis causes the return of condensate to the evaporator by centrifugal force. Fig I.4. RHP is used as heat dissipating device in rotating machinery, as cooling of gas turbine disk and blade.

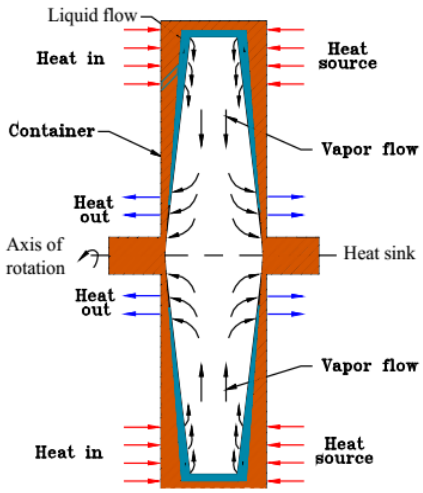

Fig I.4: Rotating heat pipe [4]

I.3.1.4. Gas-Loaded Heat Pipe (GLHP):

In GLHP , a tank containing a non-condensable gas is affixed to the condenser as shown in Fig I.5. When applying heat load to the evaporator, the internal temperature and pressure rise and lead to gas compression, and that provides a larger area of condenser section available to heat sink. By this process, the GLHP is able to maintain a nearly constant evaporator temperature regardless the applied

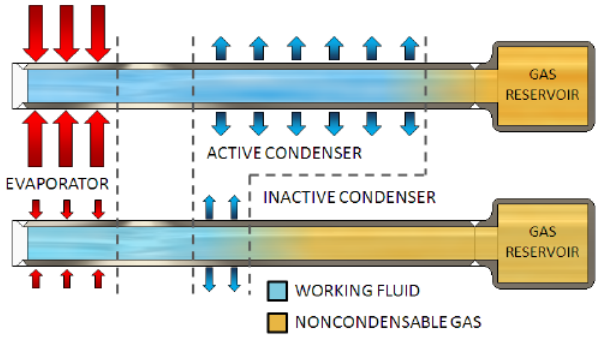

Fig I.5: Gas-loaded heat pipe [7]

I.3.1.5. Loop heat pipe (LHP):

The LHP consists of an evaporator, a compensation chamber, a condenser, liquid and vapor lines. Fig I.6. When the working fluid evaporates, the capillary force in the wick leads the vapor to move toward the condenser, where it condenses. Then the condensate flows back to the evaporator through the liquid line, by this way the process works passively and continuously. During operation, the compensation chamber stores the excess of liquid. Regarding the effectiveness of LHP to transfer heat over long distances and against the gravity, the LHP is used mostly in aerospace domain.

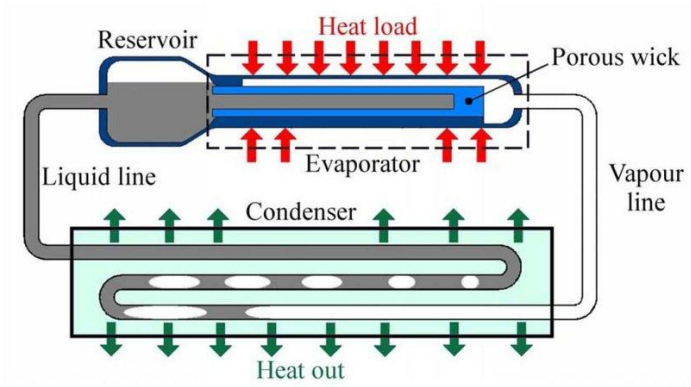

Fig I.6: Loop heat pipe [8]

I.3.1.6. Pulsating Heat Pipe (PHP):

The PHP is in from of a long tube bent into many turns. Since its diameter is very small, vapor plugs and liquid slugs are formed as a result of capillary action. Fig I.7. Heat input increases the pressure of the vapor plug in the heated section. Simultaneously, the pressure in the cooling section decreases due to condensation. This pressure difference enables the self-excited oscillatory motion of liquid slugs and vapor plugs between the two sections. PHP is used in building thermal comfort, cryogenic systems and industry.

I.3.1.7. Micro Heat Pipe (MHP):

Micro heat pipes have polygonal cross sections, with a hydraulic diameter in the range of 10-500 μm [10]. The condensate is driving by capillary forces generated in the sharp edges of the heat pipe cross section. Fig I.8.

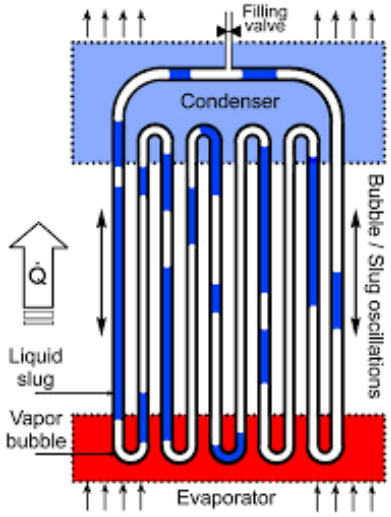

Fig I.7: Pulsating heat pipe [9]

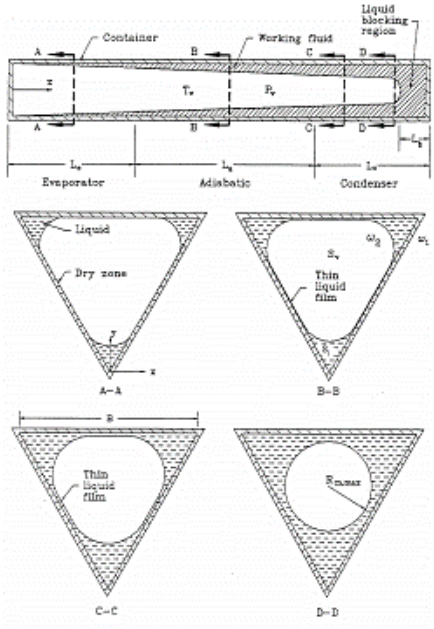

Fig I.8: Micro heat pipe [10]

I.3.2. Selection of working fluid*:*

The proper selection of working fluid plays an important role in longevity of the heat pipe. Whatever the type of the heat pipe, its design must take in consideration these points below:

- The compatibility between working fluid and container material and wick material if it exists, to avoid any chemical reaction.

- The proper choice of working fluid regarding the application temperature. Every working fluid has its own thermophysical properties that limit its working temperature range. There are four application temperature ranges as shown in Fig I.9 [4].

Some common working fluids used within heat pipes are mentioned in Table I.1 with their application temperature ranges and compatible materials.

Table I.1: Common working fluids used within heat pipes [4]

Working fluid	**Boiling Point (K) at 1 atm**	**Compatible Material**	**Range of Temperature (K)**
Water	373.1	Stainless Steel, Copper, Silica, Nickel, Titanium	303-550
Acetone	329	Aluminium, Stainless Steel, Copper, Brass, Silica	273-393
Ethanol	351	Stainless Steel, Nickel	273-403
Methanol	337	Stainless Steel, Iron, Copper, Brass, Silica, Nickel	283-403
Ammonia	240	Aluminium, Stainless Steel, Iron, Nickel	213-373
Freon 21	282	Aluminium, Iron	233-360
Potassium	1032	Stainless Steel, Inconel, Haynes	773-1273

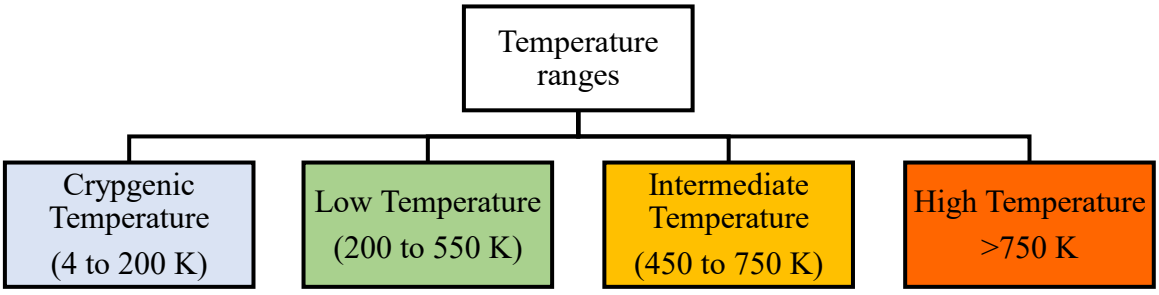

Figure I.9: Operation temperature ranges

I.3.3. The Merit Number:

The equation (I.1) below expresses the Merit number (Figure of Merit), which is an important parameter that assists in selection of working fluids regarding their thermophysical properties and application conditions. Figure shows the Merit number of some working fluids [2].

$$M = \frac{(\rho_l \sigma_l L)}{\mu_l} \quad \text{(I.1)}$$

M: Merit number (kW/m^2)

ρ_l: Density of the liquid (kg/m^3)

σ_l: Surface tension (N/m × 10^2)

μ_l: Viscosity of the liquid (PI)

L: Enthalpy of vaporization (kJ/kg)

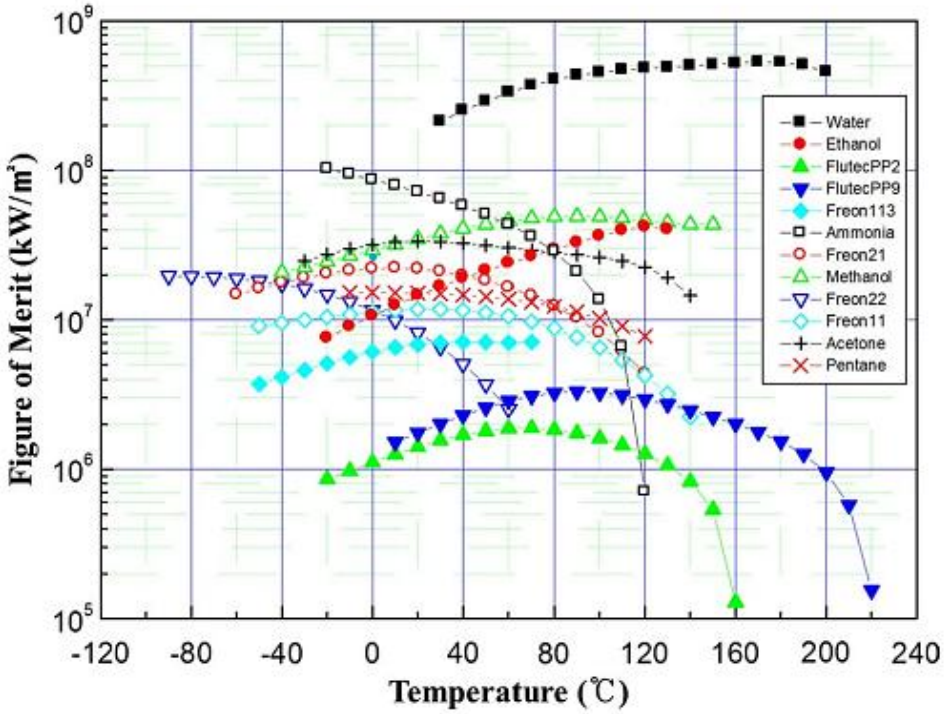

Fig I.10: Merit number of different working fluids [11]

I.4. Heat transfer mechanisms in heat pipes and its limits:

The heat transfer mechanisms within heat pipes are summarized in table I.2. The performance of heat pipes and their maximum heat flux capacity are limited due to different factors. Over the maximum heat flux, an undesirable physical phenomena may appear. Studies showed that all of parameters mentioned in Fig I.11 alter the heat transfer and thermal performance of heat pipes [12,13,14]. Thus, the inappropriate selection of these parameters can engender a serious constraint that deteriorate the device performance and even damage it. Heat pipes limits are briefly explained below.

Table I.2: Heat transfer mechanisms in heat pipes.

Mechanism	Role in Heat Pipes	Importance
Conduction	Provides the initial transfer of heat from the external source into the working fluid.	High
Convection	The phase-change convection cycle allows heat pipes to transfer large amounts of energy with minimal temperature difference.	Dominant
Radiation	Occurs between the outer surface of the pipe and its surroundings. (It is relevant in high-temperature or vacuum environments, as space applications).	Minor

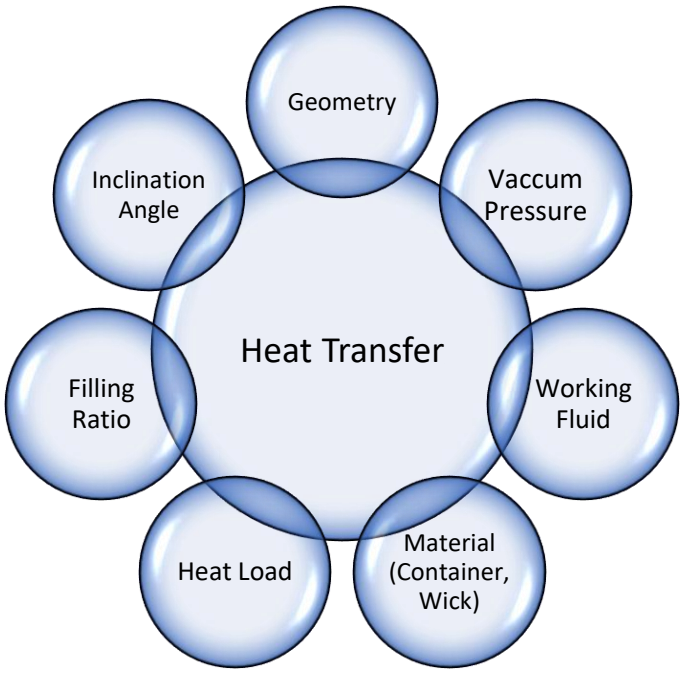

Fig I.11: Parameters influencing the heat transfer in heat pipes

I.4.1. Capillary Limit:

Capillary limit is known also as the hydrodynamic limit, it appears when the total pressure drop in heat pipe exceeds the maximum capillary pressure in the wick structure. Thus, the pumping rate becomes insufficient to pump back the liquid to the evaporator section and results a dry out.

I.4.2. Boiling Limit:

Boiling limit occurs generally when applying a high heat flux to the evaporator section, resulting a perturbated boiling regime and higher thermal resistance that lead to the dry out of the working fluid.

I.4.3. Sonic Limit:

The sonic limit is confronted when the vapor velocity reaches the sonic velocity, it can provide fissures on the container.

I.4.4. Entrainment Limit:

At high vapor velocity a strong shear forces appear at the vapor-liquid interface and consequently, liquid droplets are torn and entrained into the vapor. The vapor brings the liquid droplets to the condenser where they accumulate resulting an excess of liquid in the condenser section, and that inhibit the normal work of the heat pipe and causes a dry out in the evaporator. This phenomenon is called entrainment or flooding limit.

I.4.5. Viscous Limit:

Viscous limit or vapor pressure limit occurs when the heat pipe operates at temperature below its operating temperature range. So, the vapor pressure is not sufficient to overcome the viscous forces and consequently cannot flow from the evaporator to the condenser.

I.5. Heat transfer enhancement in heat pipes using nanofluids:

The thermal performance of heat pipe is altered strongly by the thermophysical proprieties of the working fluid, so improving the thermal potency of the working medium leads to enhance the heat transfer rate in the heat pipe. Choi and Eastman (1935) [15] proved the feasibility of enhancing the thermal conductivity of fluids by dispersion of nanoparticles within a carrier fluid. Thereafter, substitution of conventional working fluid with nanofluid was found to be an effective method to enhance the heat pipes thermal performance [16].

Nanofluid is a suspension of nanostructured materials called nanoparticles with average size of 1-100 nm in a base fluid such as deionized water, acetone or methanol. Nanoparticles could be metallic, oxide-metallic or non-metallic (Fig I.12), with different dimensions and shapes, Fig.13.

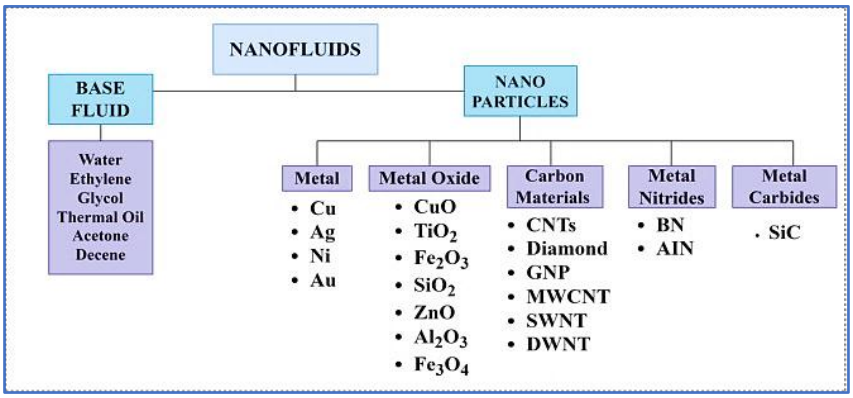

Fig I.12: Base fluids and nanoparticles used in nanofluids synthesis [17]

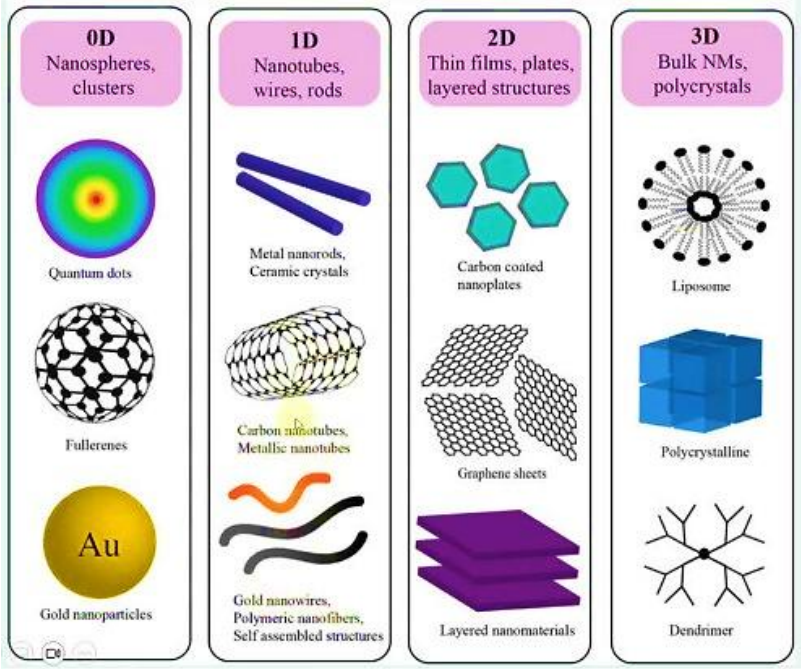

Fig I.13: Classification based dimensions of nanoparticles [18]

I.5.1. Nanofluid preparation:

Nanofluids are synthesized either using the one-step method or the two-steps method [19].

I.5.1.1. The one-step method:

This method relies on the direct mixing of base fluid and nanoparticles. There are three commonly used sub methods: (i) Direct Evaporation Method, (ii) Physical Vapor Deposition and (iii) the Liquid Chemical Method. The advantages of this techniques are the uniform dispersion, reduced agglomeration and improved stability. The drawbacks of this method are the high production time, cost and the limited application.

I.5.1.2. The two-steps method:

This two steps method of nanofluid preparation is widely used. The first step is to synthetise the nanoparticles, and the second step is to disperse these nanoparticles in the base fluid. There are three commonly used sub methods: (i) Ultrasonication process, (ii) High-pressure homogenization and (iii) Mechanical or magnetic stirring. The main drawback of this method is the nanoparticles clustering.

I.5.1.3. Nanofluids stability and stabilization methods:

Nanoparticles within the base fluid tend to agglomerate and form clusters, and sediment also due to Van der Waals interactions in between [20,21,22]. The stability of nanofluids means

the ability of nanoparticles to maintain dispersed homogenously and uniformly into the base fluid. The stability of a nanofluid strongly influences its thermal conductivity. To improve the stability of nanofluids, scientists relied on different methods such as:

- **Ultrasonication:** It is a mechanical method, represented in the breakdown of van der Waals forces between nanoparticles with help of ultrasonic waves, and that enhance the homogeneous dispersity of nanoparticles.
- **Surface modification:** It requires the anchoring of diverse materials to enhance the electrostatic repulsive charges of nanoparticles.
- **Surfactant:** Also known as "surface acting agent", it is an additive that can be added to reduce the surface tension of nanoparticles and enhance their hydrophilic properties, and to uniformly disperse the nanoparticles within base fluid. A variety of surfactants have been used for this purpose, such as: Gum Arabic (GA), sodium dodecyl sulfate (SDS), polyvinylpyrrolidone (PVP) …..etc.
- **pH controlling:** The nanofluid is considered stable when its PH value is far from Isoelectric point (IEP).

Instability causes, stability enhancement methods and mechanisms, and stability evaluation methods are summarized in Fig I.14.

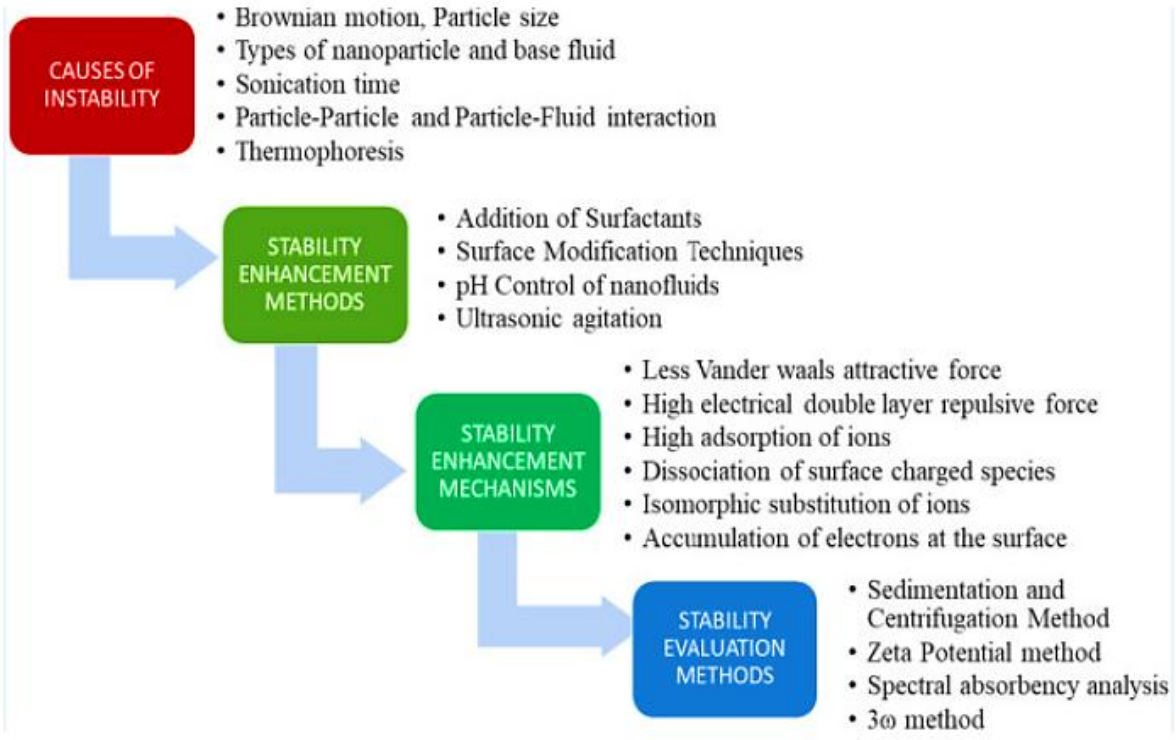

Fig I.14: Methods of stability diagnostic [23]

I.5.2. Thermophysical properties of nanofluids:

Several studies showed that the thermophysical properties of nanofluids (Thermal conductivity, Density, Viscosity and Specific heat) are influenced by several parameters such as base fluid, additives, temperature and nanoparticles characteristics (material type, size, shape and concentration). Consequently, the quality and efficacity of a given nanofluid can be enhanced or deteriorated according to those parameters [24,25,26]. Numerous models and approaches available in literature were used to predict the thermophysical properties of nanofluids.

I.5.2.1. Thermal conductivity of nanofluids

Thermal conductivity is a heat transfer property which can be defined as the ratio of heat flux to a local temperature gradient. Many empirical correlations were developed for thermal conductivity of nanofluids after performing various theoretical and experimental studies with specified types of nanofluids, considering their chemical properties and geometric parameters of nanoparticles.

As a nanofluid contains substances with different phases (solid and liquid), it was necessary to develop a novel correlations and measurement techniques. The first correlation to compute nanofluids thermal conductivity, was presented by Maxwell (1873), equation.2 [27]. However, this correlation was only applicable to spherical nanoparticles. Latterly, other correlations for non-spherical nanoparticles were developed by other researchers.

$$k_{nf} = \frac{k_p + 2k_{bf} + 2(k_p - k_{bf})\Phi}{k_p + 2k_{bf} - 2(k_p - k_{bf})\Phi} k_{bf} \quad \text{(I.2)}$$

I.5.2.2. Density of nanofluids

Incorporation of nanoparticles in base fluid changes all of friction factor, pressure loss, Nusselt and Reynolds numbers. Consequently, it alters the heat transfer and flow patterns of the base fluid. Studies proved that, as the difference between nanoparticles and base fluid is large, as the sedimentation will occur within the suspension.

The density of a suspension has a relation with concentration of nanoparticles. Vsajjha et al.(2009) developed a simple correlation for nanofluids density equation.3 [28].

$$\rho_{nf} = \Phi\rho_p + (1-\Phi)\rho_{bf} \quad \text{(I.3)}$$

I.5.2.3. Viscosity of nanofluids

Base fluids are Newtonian fluids such as water. Addition of nanoparticles augments the viscosity of base fluid, because solid nanoparticles disrupt the velocity profile of the base fluid. The analytical model for solid liquid suspension was derived by Einstein in 1906 [29], its correlation is the follow:

$$\frac{\mu_{n_f}}{\mu_{bf}} = 1 + 2.5\Phi \quad \text{(I.4)}$$

Latterly, this model was developed to include the influence of spherical nanoparticles on fluid velocity lines and Brownian motion effect.

I.5.2.4. Specific heat of nanofluids

Specific heat capacity is a critical thermodynamic property of a material. It represents the amount of heat required per mass unit to raise with one degree the temperature.
It reflects the thermal characteristics and performance of any material. The specific heat capacity of nanofluids can either be low or high compared to base fluids, depending on several parameters, as the thermal conductivity does. Equation.5 represents the specific heat capacity correlation [30].

$$C_{P,n_f} = \frac{(1-\Phi)\rho_{bf}\cdot C_{p,bf} + \Phi\cdot\rho_p(c_{p,p})}{\Phi\cdot\rho_p + (1-\Phi)\cdot\rho_{bf}} \quad \text{(I.5)}$$

I.5.3. General impact of nanofluids on heat pipes:

Since Chien et al. [31] published the first research paper about the application of nanofluids in heat pipe, a huge number of experimental and numerical investigations have been conducted on different types of heat pipe using nanofluids. The table I.3 below summarizes some research that contributed to reveal the impact of nanofluids on different heat pipes using various nanofluids. According to the literature, adding nanoparticles to the base fluid with optimal concentration enhance its thermal capacity to transfer heat and this positive impact is

represented mainly in lower total thermal resistance and higher heat sink in heat pipes. The behaviour of nanoparticles and mechanisms of heat transfer in nanofluids are controversial, although the implementation of nanofluids in heat pipes represents an effective solution to enhance their thermal performance, but high cost and stability issues still standing out.

Table I.3: Important findings of studies performed on heat pipe using nanofluids

Ref	Heat Pipe	NP/Base Fluid	Concentration	NP size	Operation Condition	Impact on Heat pipe
[32]	Conventional heat pipe (Mesh wick)	CuO/DI	0.5, 1.0 and 1.5 wt.%	40 nm	Inclination angles: 30°, 45°, 60°, 75° and 90° Heat Load:10 –140 W	Thermal efficiency increased by 31.87% for 1.0 wt.%.
[33]	Conventional heat pipe (Sintered)	CuO/DI	0.5, 1.0 and 1.5 wt.%	39.1 nm	Heat load: 10–160 W Inclination angles: 0°, 30°, 45°, 60°, 75°,90°	Thermal resistance reduced by 66.1% and the thermal efficiency is increased by 24.9%.
[34]	Conventional heat pipe (Grooved)	Al_2O_3/DW	3 vol.%	20 nm	Inclination angles: 0°,30°,60°,90° Filling ratio: 20, 40, 60 and 80% Heat load: 45 W, 65 W	The HTCs of evaporation and condensation increased by 30.4%and 11.1%, respectively. The thermal resistance decreased by 18.2%.
[35]	Conventional heat pipe (Grooved)	CeO_2:MWCNT/DI	0.25–1.50 vol.% (80: 20)	CeO_2:<30nm MWCNT: (Ø: 20 nm, L:1–20 µm)	Surfactant: CTAB Operation temperature: 55–75°C	The heat transfer capacity increased by 61.27% and the total thermal resistance is reduced by 30%.
[36]	TPCT	Al_2O_3:Cu:TiO_2/DI	0.1, 0.3, 0.5 vol.% (4:2:4)	20 nm,30 nm,50 nm	Dispersant: PVP Heat load:40, 60, 80 W Inclination angles: 30°,60°,90°,120°, 150°	Thermal efficiency enhanced by 22% with 0.3% at 80W and 90°.
[37]	TPCT	Ag/DI	0.1,0.2,0.3,0.4 wt.%	40–60 nm	Heat load: 80–600 W Filling ratio:25-80% Inclination angles: 0°,20°,40°,55°, 60°	Temperature distribution profile along the heat pipe was reduced. The best thermal performance is reported with 0.4 wt.% at FR of 65% and inclination of 55°
[38]	Rotating heat pipe	Cu/water CuO/Water Al_2O_3	0.04 vol.%	5 nm	ΔT = 20 °C ω = 3000 rpm	The maximum heat transfer increased by 56%.
[39]	Loop heat pipe	graphene nanosheets/ DW	0.003, 0.006 and 0.009 vol.%	1–5 nm thickness	Heat load: 20–380 W Filling ratio: 30%	Thermal resistance reduced by 21.6%. The evaporator interface temperature decreased by 10.3 °C with concentration of 0.006%
[40]	Pulsating heat pipe	MWCNT/DW	0.05, 0.1, 0.2 and 0.3 wt.%	Ø: 20 nm L: 5 µm	Heat load: 50–400 W Filling ratio: 60%	Best thermal performance with 0.2 wt.%.
[41]	Micro heat pipe	Al_2O_3/DI	0.1, 1.1%	38.4 nm	Heat load: 0–110 W	Thermal performance improved up to 100% with concentration less than 1.0%. Thermal resistance decreased with increasing nanoparticles size.

I.6. Conclusion:

This chapter broached a general view on heat pipes and their importance in nowadays technologies, which allows to the reader to recognize heat pipes field, and the concept of using nanofluids within to enhance their thermal performance.

CHAPTER II

State Of The Art On Thermosyphons Using Nanofluids

II.1. Introduction

The previous chapter gave a general view on heat pipes and their heat transfer enhancement using nanofluids. Regarding the prospective study, this chapter represents a state of the art on the gravity assisted wickless heat pipe, also called two-phase closed thermosyphon (TPCT). The TPCT applications, challenges, phase change schemes and overview on TPCT using nanofluids are available in this sequence.

II.2. TPCT application Fields

As all heat pipes, The TPCT uses phase change phenomenon to ensure the passive heat transfer and cooling. The essential difference between a conventional heat pipe and a TPCT is that the latter use the gravitational force instead of the capillary force to return of the condensate to the heated region, as mentioned in Fig I.3 in the precedent chapter According to application needs, the TPCT can be in form of a loop, L shape or containing multiple evaporators and condensers. Due to its efficacity, design simplicity and flexibility with low-cost manufacturing compared to other heat pipes, it is implemented in various thermal management systems. such as HVAC systems, flow plates cooling for fuel cells, electronic systems, air to air heat exchangers, de-icing of roadways in permafrost regions, solar collectors and nuclear reactors. Some of application scopes are explained below.

II.2.1. TPCT application in solar collectors

The thermosyphon evacuated tube solar collector converts solar energy to heat energy. It consists of a vacuum tube and a TPCT. Vacuum tube is made of two concentric glass tubes, in which the outer surface of the inner tube is coated with a selective absorber material to convert the absorbed solar radiation to heat energy, and also reduce the radiation heat loss. The absorbed heat in the vacuum tube is transferred to the evaporator section of the TPCT and released by the condenser section. By this passive process, the water traversing the tank above can be heated continuously and used for houses or industry’s needs.

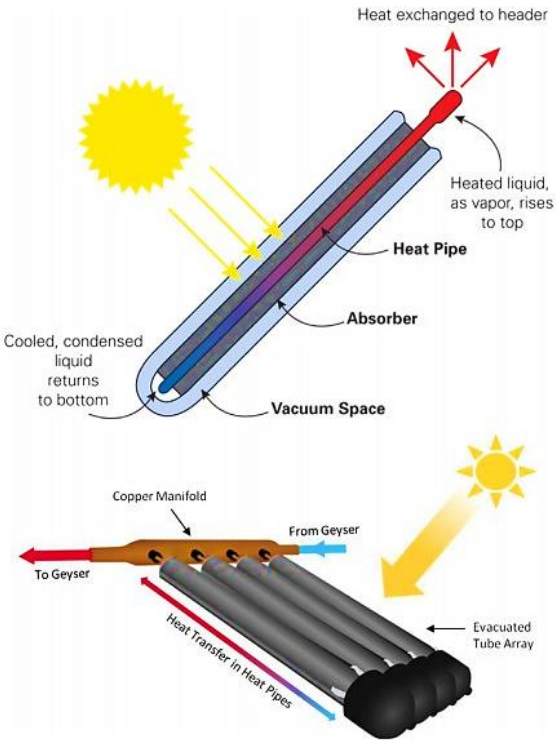

Fig II.1: Schematic view of thermosyphon evacuated tube solar collector [42]

II.2.2. TPCT application in permafrost regions:

Permafrost is the ground that remains completely frozen with 0°C or colder continuously for two years at least. Permafrost regions span approximately 25% of the ground in the northern hemisphere of the earth, mainly Canada, China, Russia and USA as represented in Fig II.2.

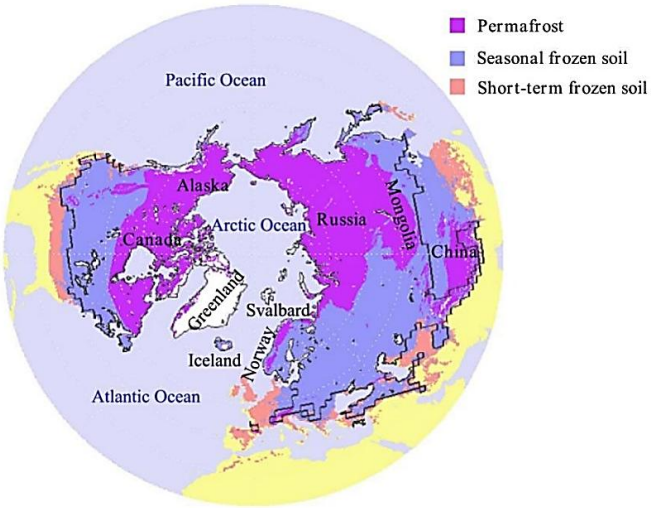

Fig.2: Distribution of permafrost in the northern hemisphere [43]

Over a long period, scientists have been industriously attempting to resolve the issue of damage to highway pavements in permafrost regions. They realized that the TPCT can prevent to some extent the permafrost degradation, and then it was adopted on highways and railways sides as shown in Fig II.3.

(a) Gonghe-Yushu Highway (b) Qinghai-Tibet railway

Fig II.3: Application of TPCTs in Permafrost regions [44]

The condenser section is exposed to the air and the evaporator section is inserted underground as shown in Fig II.4. The TPCT can effectively transport a large amount of heat with a small temperature difference between the condenser section and the evaporator section.

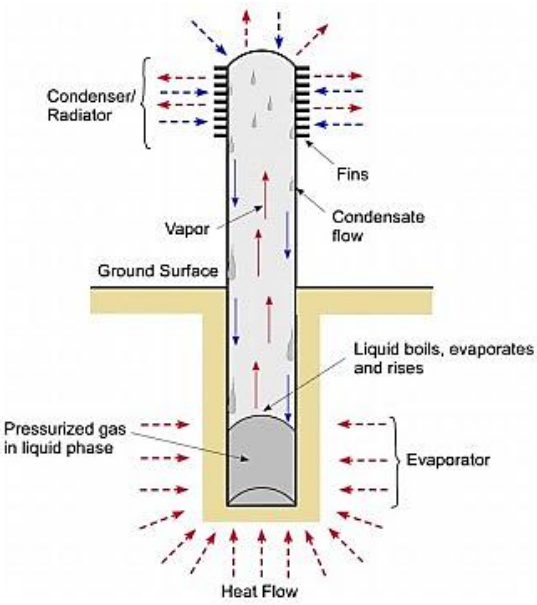

Fig II.4: Distribution of permafrost in the northern hemisphere [45]

II.2.3. TPCT application in heat exchanger for heat waste recovery systems

In this technology, a bunch of TPCTs are placed into a shell called recuperators, in which the TPCTs sections are isolated from each other. The hot exhaust fluid passes through the bottom of TPCTs heating the evaporator. Thereafter, the heat is released on the top part by condensers and heats the cold fluid, as explained in Fig II.5. This heat waste recovery system is widely used in various industrial domains.

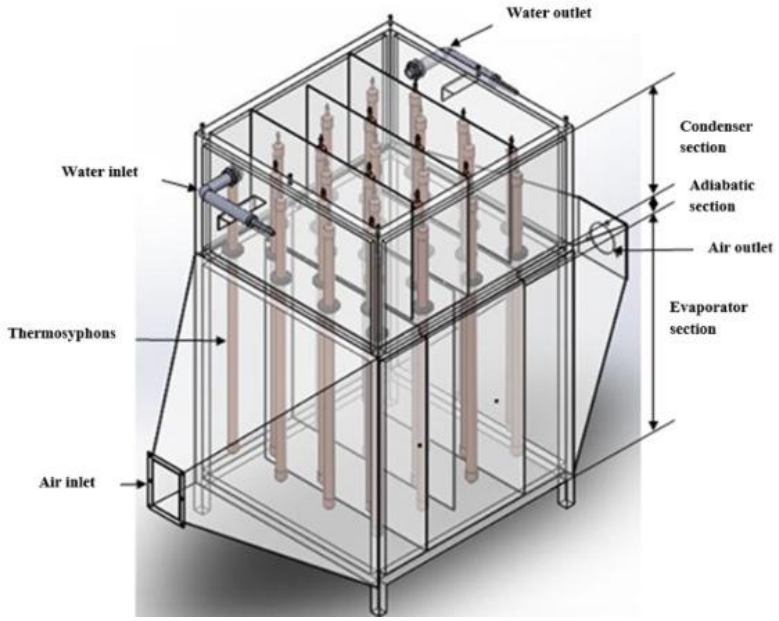

Fig II.5: A schematic view of the thermosyphon heat exchanger [46]

II.3. Physical concepts of heat transfer in TPCT

II.3.1. Boiling in TPCT

The TPCT is fulfilled with an amount of working fluid which takes place in the bottom of the tube. Before boiling starts, the working fluid is in stationary regime representing the liquid pool in the TPCT. After applying the heat to the evaporator section, heat is transferred from the inner wall surface to the bulk liquid via natural convection. Thereafter, typical boiling regimes occur as shown in Nukiyama's boiling curve for saturated pool boiling of water at atmospheric pressure, Fig II.6. Ranges of boiling temperatures vary mainly according to vacuum pressure, working fluid nature and tube material [47].

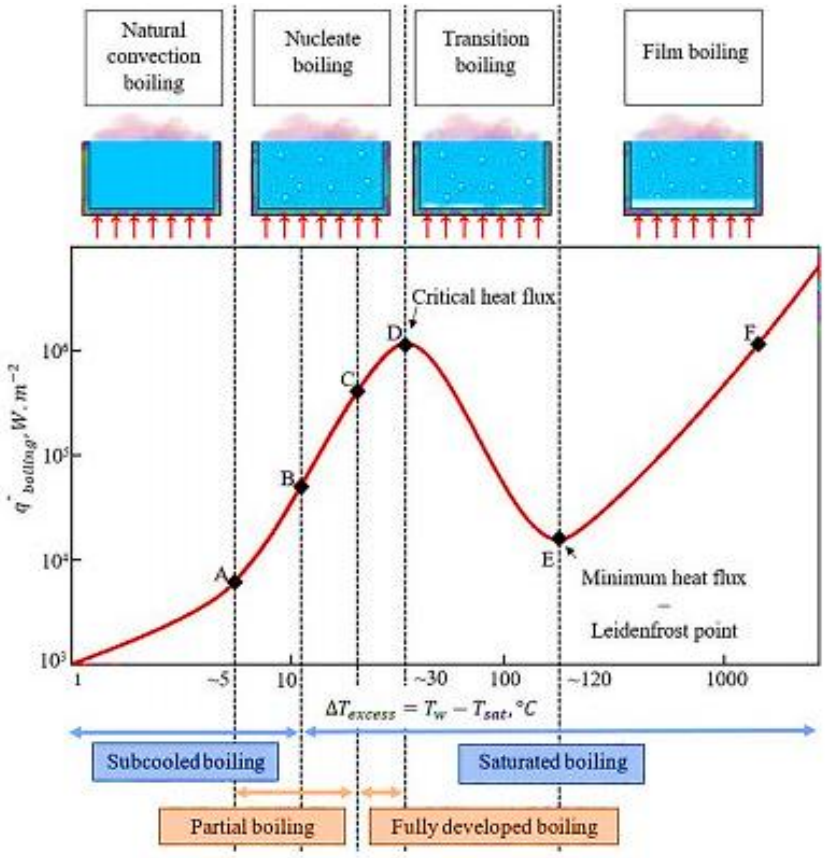

Fig II.6: Pool boiling curve of saturated water [47]

II.3.1.1. Naturel convection boiling:

In natural convection boiling regime, the bulk liquid is subcooled with no bubbles generation As the temperature increases, few bubbles may generate near the evaporator inner wall. The only fluid motion in the pool is caused by natural convection currents, which are triggered by a change in fluid density due to temperature increment. Since the boiling heat transfer coefficients are low in natural convection regime, this last one has not gained much of scientists attention.

II.3.1.2. Nucleate boiling:

When the system enters the nucleate boiling regime, vapor bubbles occur on the evaporator inner wall at certain locations called nucleation sites, these are microscopic cracks or cavities on the wall surface. The existence of trapped gases in cavities produces liquid–vapor interfaces, where transfer of energy occurs in form of latent heat from the liquid to the vapor. Once a vapor bubble generates at a nucleation site, the bubble grows to a certain diameter, detaches from the wall, and departs to the liquid bulk. Bubble growth steps are represented in Fig II.7.

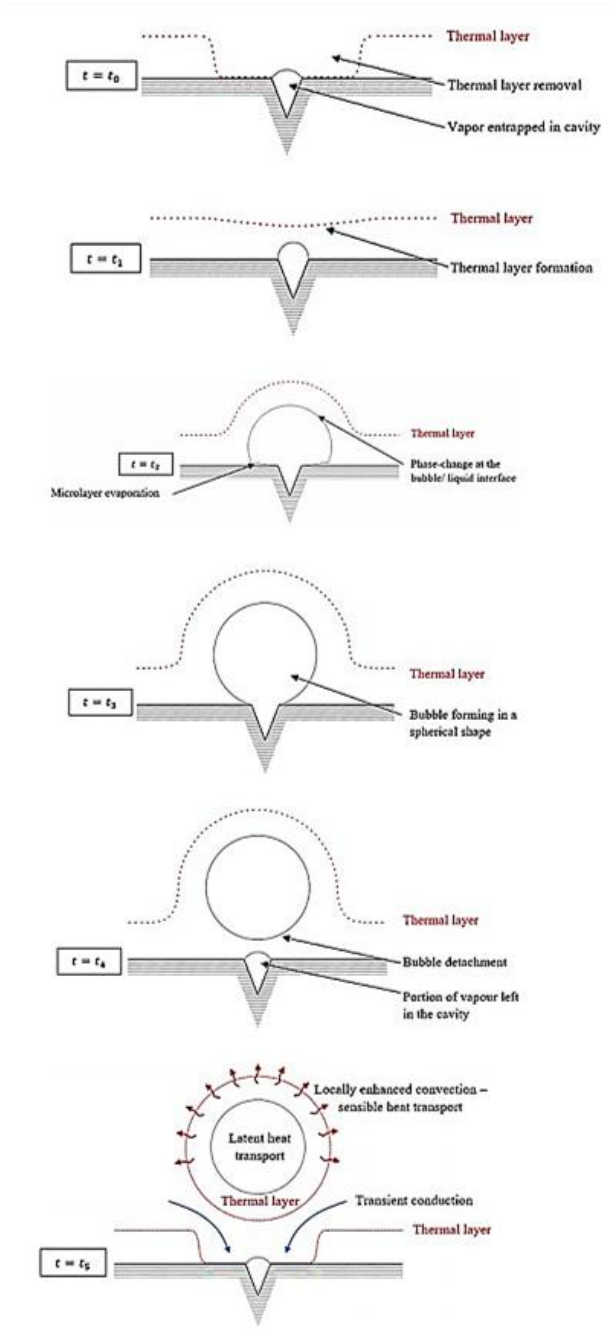

Fig II.7: A bubble growth and detachment steps [47]

At subcooled region, each generated bubble can grow and detach from the surface independently, this is called “isolated bubble” regime. As the temperature rises, additional nucleation sites become active and more bubbles are generated, and then interact with each other forming columns and slugs of vapor, which decreases the contact area between the heating surface and the saturated liquid.

In some cases, at low pressure and low filling ration, the vapor bubble growth further the average diameter of detachment, due to the imbalance of forces surrounding the bubble; and that results an anomalous nucleate boiling appearance, and this phenomenon is called geyser boiling. Phases of geyser boiling occurrence are explained below (See also, Fig II.8 and Fig II.9).

- The vapor bubble is nucleated and enlarges suddenly, than it reaches the pool liquid-vapor interface, and it bursts.
- The proximate liquid to the bubble is sprayed over the condenser inner wall due to bubble rush. Consequently, a liquid slug forms and bashes the condenser end cap.
- Thereafter, the bashed liquid returns to the pool by gravity force. The falling liquid returns with a lower temperature and cools the liquid pool in the evaporator.
- After the large bubble is burst, the new nucleated bubbles are smaller and release less energy than the large one. Eventually, liquid pool returns to a state of relaxation and a new geyser boiling cycle begins.

Geyser boiling influences the thermal performance of the TPCT due to the produced instabilities, represented in relaxation periods followed by abrupt nucleation.

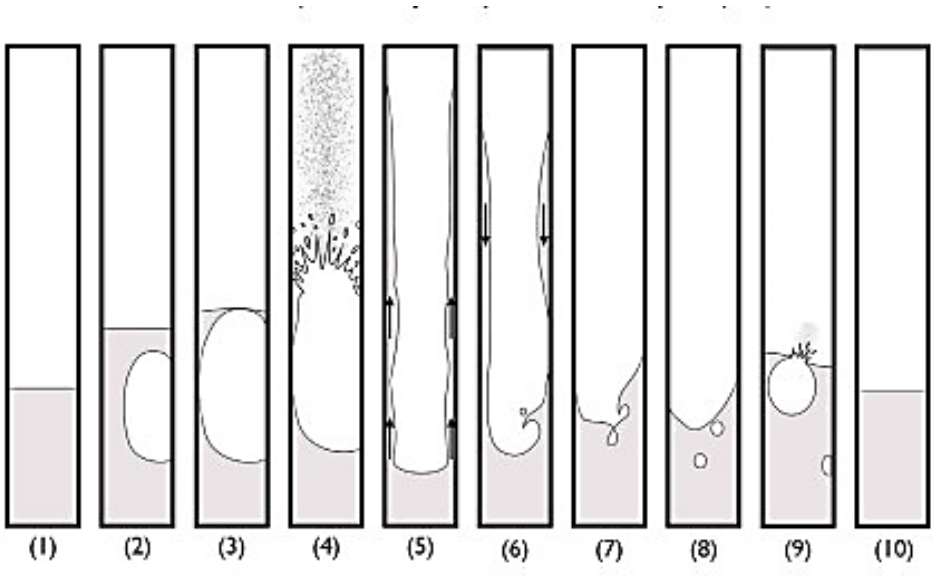

Fig II.8: Phenomenology of geyser boiling in the TPCT [48]

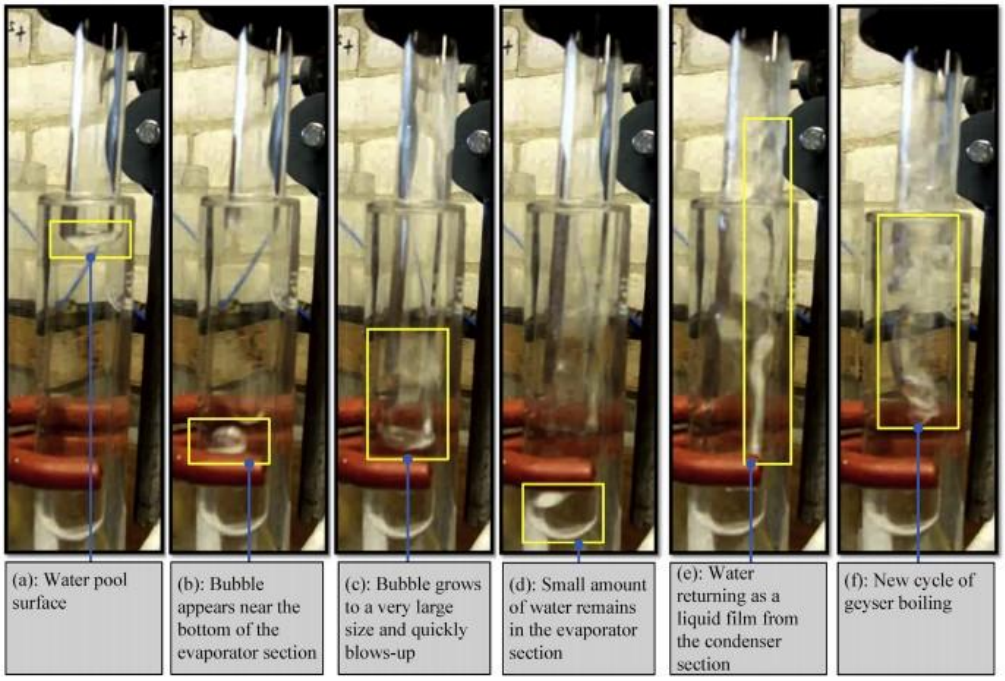

Fig II.9: Geyser boiling visualistaion through a glass thermosyphon [49]

II.3.1.3. Transition boiling

When the temperature rises over the critical heat flux point, the rate of bubble formation outpaces the rate of bubble detachment from the solid surface.Bubbles combine and form vapor films on the solid surface, so the contact area between the solid surface and the saturated liquid decreases. The formed vapor films are not stable, and they can separate from the surface, leading to put back the contact with the liquid and restart of nucleate boiling. This causes instability of solid surface temperature in which the temperature may fluctuate quickly. Since this regime fuses unstable film formation with partial nucleate boiling, it is defined as transition boiling regime.

II.3.1.4. Film boiling

At Leidenfrost point, the heat flux reaches its minimum value, in where the temperature becomes sufficiently high to maintain a stable vapor film. Above this point , the stable vapor film separates completely the bulk liquid and the solid surface, and that why it is called film boiling regime. In this regime, Thermal energy from the heating surface reaches the liquid–vapor interface by convection in the vapor film as well as by direct radiation to the interface.

Film boiling manifests until the surface temperature reaches the maximum admissible temperature, which is the melting point of the solid surface.

II.3.2. Evaporation in TPCT

Evaporation is the transformation of a liquid to vapor phase; this process occurs at liquid–vapor interface. In TPCT, Evaporation process occurs firstly at the top of liquid pool. The released vapor traverses the adiabatic section and moves towards the condenser section where it changes phase to liquid by releasing its latent heat of condensation. When the condensate falls down due to gravity, evaporation take place also on the adiabatic wall where the liquid films or droplets vaporize. Fig II.10 below illustrates vapor flow patterns in the TPCT. Manifestation and frequency of these flow patterns differ according to various parameters.

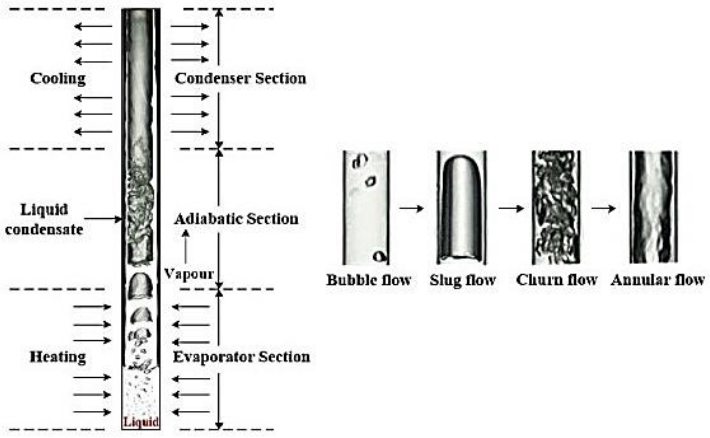

Fig II.10: Illustration of vapor flow patterns in the TPCT [50]

II.3.3. Condensation in TPCT

Condensation happens when the saturated or superheated vapor comes into contact with a solid surface, which has a temperature less than its saturation temperature, such as the inner wall of condenser section in the TPCT. It exists two condensation modes, which are explained below and figured in Fig II.11.

II.3.3.1. Filmwise Condensation

When the surface is wettable, a continuous condensate film forms on the surface and filmwise condensation manifests, Fig II.11 (a). Filmwise flow could be laminar, wavy or turbulent. Filmwise is characterized by its width and thickness.

II.3.3.2. Dropwise Condensation

Dropwise condensation is a heterogeneous phase change process, in which vapor transforms to liquid in form of small discrete droplets on a non-wettable surface, as shown in Fig II.11 (b). These droplets can coalesce and move down due to gravity sweeping the condenser.

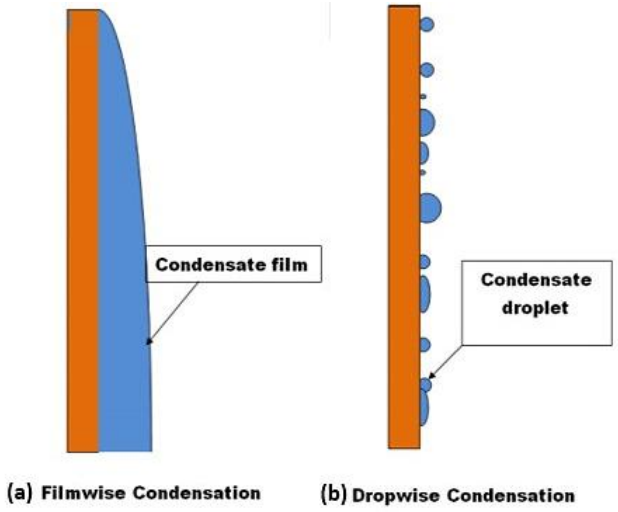

Fig II.11: Condensation modes [51]

In the TPCT, the dropwise condensation is preferred, because its overall heat transfer coefficient is higher. With filmwise condensation, the inner wall of condenser section is covered permanently with a thin film, and whatever its flow regime is, it engenders a supplementary thermal resistance and decreases the heat transfer rate. Unlikely, with dropwise condensation the inner wall of condenser section has much bare area not covered, which reduces the thermal resistances encountered at the liquid–vapor interface. Scientists work on promoting dropwise condensation in TPCT by coating condenser inner surface with hydrophobic impurities, known as dropwise promoters.

Seo et al [52], demonstrated that the dropwise condensation for acetone and ethanol reduced the overall thermal resistance by 50% compared to filmwise condensation, as represented in Fig II.12. Furthermore, their work revealed that it exists a strong dependence of working fluid viscosity on dropwise condensation stability and heat transfer enhancement. The high viscosity of working fluid delayed the droplets shedding rate, and that engenders coalescence of droplets, resulting an irregular and wide transient liquid film. Consequently, the condensation rate and heat transfer performance decrease.

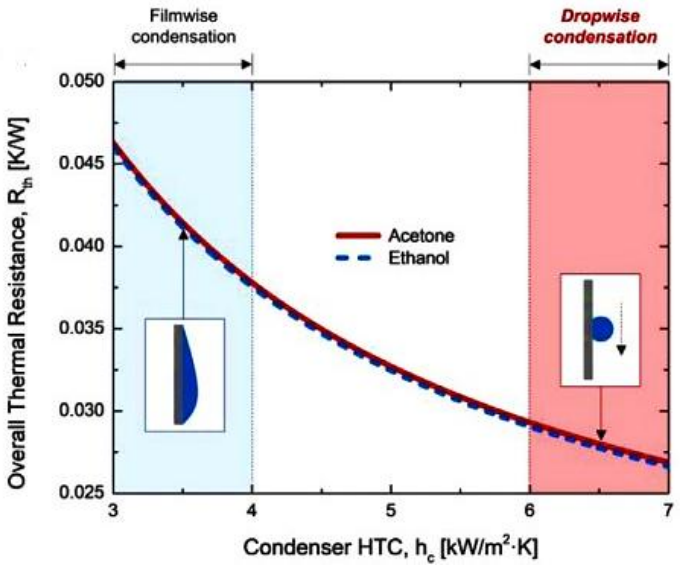

Fig II.12: The overall thermal resistance of a TPCT as a function of the CHTC [52]

II.4. Heat transfer limits in the TPCT:

Previously, the limitations of heat pipes were defined. Since the TPCT is a wickless gravity assisted heat pipe, it is not limited with capillary force. The TPCT is mainly limited by boiling and entrainment limits, which both of these limits engender the dry out of the evaporator and consequently the device damaging. Studies have shown that different parameters have significant impact of the TPCT thermal performance, such as: Effective length, diameter, inclination angle, material, working fluid, filling ratio, heat flux.

It was figured out that adding nanoparticles to a base fluid alters its thermophysical properties and therefore the phase change regimes and subsequently the TPCT performance [53]. Moreover, many studies demonstrated that filling ratio which is defined as the volume of the working fluid to the evaporator section volume, has a significant impact on TPCT performance. The next section will browse various works conducted to investigate both filling ratio and nanoparticles addition impact on thermal performance of the TPCT.

II.5. Overall Heat transfer enhancement using nanofluids

A variety of experimental and numerical studies have been conducted to reveal the effect of nanofluids with different filling ratios on the thermal behaviour of thermosyphons. Main results and remarks are briefly mentioned below.

Gallego et al. [54], used a glass TPCT with length of 400 mm to visualize phase change progress when using deionized water and alumina nanofluid with 0.1 wt.% and 0.5 wt.% of concentration, and filling ratios of 30, 45, 60, 75 and 90% at 40, 60 and 80 W. It was noticed that using Al_2O_3/DI nanofluids at 0.1 wt.% and 0.5 wt.% eliminated the dry out limit of the TPCT and reduced the condenser temperature. With filling ratios above 45%, nucleate pool boiling occurred with a remarkable expansion of the working fluid. In addition, a nanoparticle barrier appeared with concentration of 0.5 wt.% at 40 W. This phenomena impeded the vapor from moving towards the condenser, which caused a supplementary thermal resistance and deteriorated the thermal performance of the TPCT compared to its performance with water. Adding of Al_2O_3 nanoparticles with concentration of 0.1 wt.% with FR of 45% at 60 W, decreased the thermal resistance by 30.5%, while 0.5 wt. % decreased it just with 25.8%. those findings, show that it exists a relation between all of heat load, filling ratio and nanoparticles concentration.

Sarafraz et al [55], used Ag/water nanofluid in a copper TPCT with total length of 280 mm. The nanofluid was prepared by dispersing in water an eco-friendly silver nanoparticles which were produced from the aqueous silver nitrate and the fresh tea leaf extract. Ag/water nanofluids decreased the wall in a temperature distribution profile along the TPCT, and its best performance was reported at 0.4 wt.% of concentration and FR of 65% at vertical position.

In the same TPCT, Sarafraz et al [56] conducted another study using Zirconia-acetone nanofluid. Nanoparticles concentration varied from 0.025 wt.% to 0.1 wt.%, and it was found that as the concentration increases as the thermal resistance and wall temperature decrease. The optimum filling ratio and nanoparticles concentration values was found to be 60% and 0.1 wt.%, respectively. In which the heat transfer coefficient of the TPCT improved by 36.3% in comparison with the pure acetone.

Effect of single and hybrid nanofluids of Al_2O_3 and TiO_2 were investigated with concentration of 0.2 vol. % and FR of 30, 50, 70% on carbon steel TPCT with length of 500 mm [57], where 25% Al_2O_3 + 75% TiO_2- H_2O and TiO_2-H_2O nanofluids showed the best performance represented in lower thermal resistance with 26.8% and 22.8%, higher heat transfer coefficient and better thermal efficiency. Whereas the optimum FR was found to be 50%.

Al_2O_3 and Bimetallic nanoparticles of Titanium Silicon oxide $TiSiO_4$ nanofluids with various concentrations (0.01%, 0.02%, 0.05% and 0.075%), were used within a copper TPCT [58]. Both nanofluids decreased the overall wall temperature and thermal resistance compared to pure water. Optimum concentrations are 0.05 vol.% and 0.075 vol.% for Al_2O_3 and TiSiO4, respectively.

Different numerical approaches of computational fluid dynamics with different assumptions have been applied to predict the impact of nanoparticles on TPCT thermal performance. Asmaie et al [59], developed a computational fluid dynamics model for simulation of a TPCT including phase change. Results showed that the evaporator wall temperature decreased about 19.6% when using Cu/H_2O nanofluid from 0.1 to 1 wt. %. A mathematical 2D steady state model was developed by Wang et al [60] to explore the effects of nanoparticles on a TPCT charged with nanofluids. Wall temperature distribution decreased by 3.92%, 4.54%, and 5.83% for Al_2O_3, Fe_2O_3, and Cu, respectively for 10 wt. % and FR 35%.

In addition to metallic and oxide-metallic nanoparticles, non-metallic nanoparticles have been also investigated. Liu et al. [61], used a miniature TPCT with carbon nanotubes suspensions CNT/H_2O as working fluid. The thermal resistance decreased with the increase of CNT concentration and the greatest heat transfer coefficient was accessed at 2 wt. %.

Baek et al. [62], utilized functionalized multi walled carbon nanotubes (MWCNTs) with five filling ratios, 10%, 30%, 50% and 70% in distilled water. Both of M-CNT and C-CNT nanofluids decreased the thermal resistance and increased the heat transfer coefficient, especially with FR 10% at 8W. It was clearly remarked that M-CNT nanofluid enhanced the thermal performance of the TPCT better than C-CNT nanofluid and deionized water.

Only Zhao et al. [63] studied the effect of nanofluid on the startup of two-phase closed thermosyphon. They used Graphene nanoplatelets nanofluid with different concentration. Using 0.05 wt. % of GNPs nanofluid, shortened the startup by 15.1% at 30 W. Meanwhile, the temperature of the startup process decreased by 3.7%. They concluded also that the shorter startup is, the higher thermal efficiency is.

Choi et al. [64], performed a wire pool boiling experiment for the purpose of determining an optimal concentration of CNF within water. Aggregation and sedimentation were not remarked, even after repeated experiments over a long duration, which implies the good stability of the suspension. Thereafter, CNF fluid of 0.5 wt. % concentration was used as working fluid within

the TPCT with three different filling ratios and various heat loads. The maximum reduction rate in thermal resistance was 37.7% at 25% of filling ratio.

In other supplementary work, Choi et al. [65] repeated the experiments on the same TPCT with the same conditions and using an evaporator with hydrophilic inner surface. It was found that using CNF nanofluid reduced the thermal resistance and improved dramatically the TPCT thermal performance. Lee et al. [66], extended these last two studies by analysing the flow instability at the evaporator section. It was figured out that CNF reduced the amplitude of geyser boiling that causes the instability of the TPCT.

II.6. Behaviour of nanoparticles in TPCT using nanofluids

The behaviour of nanoparticles in base fluid during the operation of the TPCT is unexpectable. After literature survey, three main behaviours were referred to the ability of nanoparticles to enhance the thermal characteristics of base fluids. All of Brownian motion, interfacial nanolayers formation and deposition of nanoparticles are explained in the following section.

II.6.1. Brownian motion of nanoparticles:

With aim to fathom the role of Brownian motion of nanoparticles in heat transfer, two theoretical models were proposed, dynamic or static models. Maxwell [67] and Hamilton and Crosser [68] proposed static models. They assumed that the nanoparticles are stationary in the base fluid. while other researchers proposed dynamic models, in which the nanoparticles are assumed to be in a random movement within the base fluid. Goudarzi et al [69] and Harish et al [70] figured out that Brownian motion has a significant impact on thermal conductivity enhancement in nanofluids. Jang and Choi [71] developed a dynamic model, where they introduced four concepts of energy transfer in nanofluids, which are: thermal diffusion, the collision of base fluid molecules, thermal interaction between nanoparticles and base fluid and collision between nanoparticles. The study concluded that the collision between nanoparticles (Brownian motion) of nanoparticles has not a significant role in enhancing the thermal conductivity of the nanofluid. According to Borzuei and Baniamerian [72] the only effect of

convection due to Brownian motion of nanoparticles is able to explain the high thermal conductivity enhancement in nanofluids.

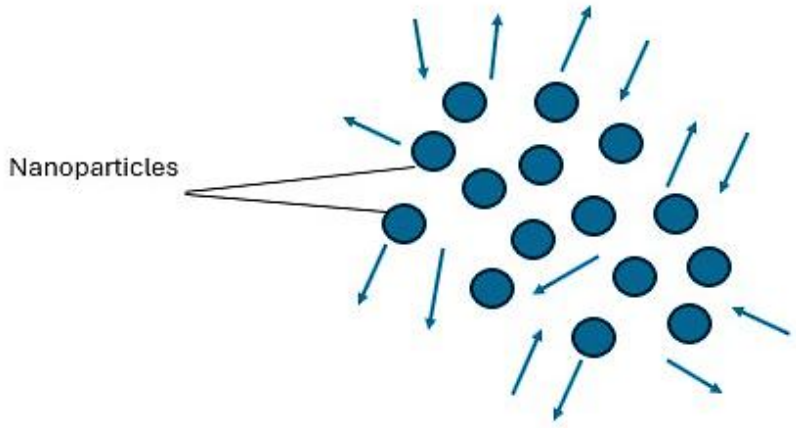

Fig II.13: Nanoparticles in random movement (Brownian motion)

It is clear that findings of theoretical studies about Brownian motion role in heat transfer in nanofluids are contradictory. However, visualisation experiments have shown that the random movement of nanoparticles bombards the vapor bubbles formed in the working fluid bulk in the evaporator section during the nucleate boiling, and also bombards the nucleation sites. Thus, frequency of bubbles generation increases, and smaller bubbles. This results higher energy transfer and reduction of the thermal resistance.

II.6.2. Interfacial nanolayers formation:

Within nanofluids liquid molecules wraps around nanoparticles forming a nanolayer (Fig II.14), this one is supposed to be a thermal conductor between the nanoparticles and the base fluid and helps enhancing the thermal conductivity of the nanofluid. Li et al [73] and Zhai et al [74], reported that the nanolayer thickness is not a parameter that to determine the thermal conductivity.

Contrary to the finding mentioned above, Pal [75] came up with a novel method to estimate the thermal conductivity of the interfacial nanolayers surrounding the nanoparticles. The method consists of measuring intrinsic viscosity of the bulk which allows to estimate the thickness of the interfacial nanolayers. Thereafter, with help of the developed equations relating

intrinsic viscosity to interfacial layer thickness and intrinsic thermal conductivity to interfacial properties, the thermal conductivity of the nanofluid can ben deduced. This method was validated by simulation and experimental results.

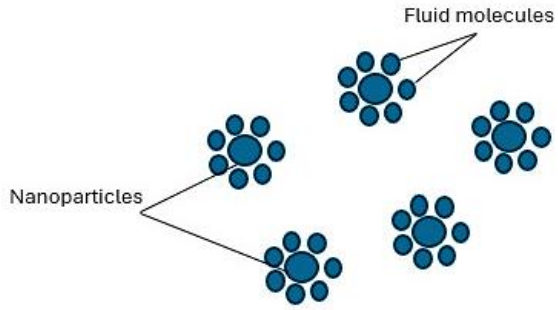

Fig II.14: Nanolayers at liquid-solid interfaces

II.6.3. Deposition of nanoparticles :

Additionally, even with stable suspension, an amount of nanoparticles within the nanofluid tend to depos on the inner wall of evaporator section, forming a thin layer. This layer promotes the roughness and cavities of the surface, which can potentially boost the number of nucleation sites. Sarafraz et al [76], studied heat transfer in evacuated tube solar collector using carbon-acetone nanofluid. They took SEM images for evaporator inner wall after continuous operation with nanofluid. the change of surface roughness due to deposition of nanoparticles on the surface is clearly obvious. Irregularities and the non-uniformity of the surface intensified with rise of nanoparticles concentration, Fig II.15.

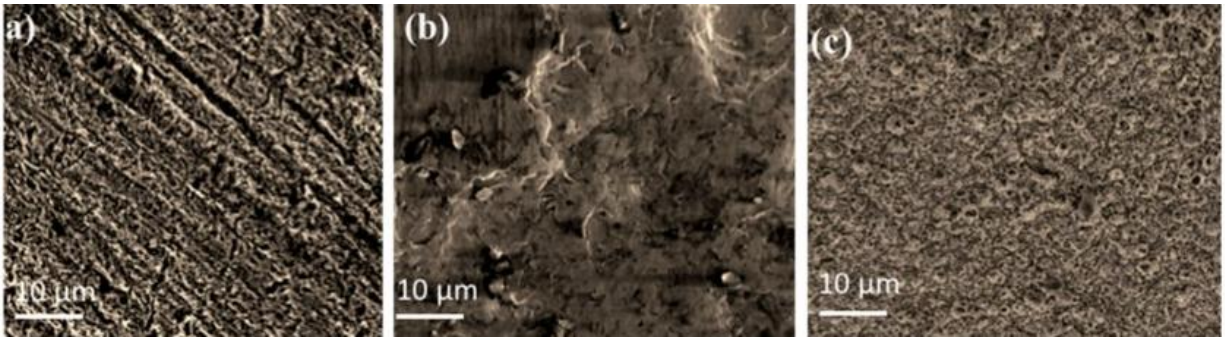

Fig II.15: SEM images taken from the evaporator after continuous operation with nanofluid (**a**) 0.025 wt.% (**b**) 0.075 wt.% (**c**) clean surface [76]

II.7. Conclusion

This chapter focused on the Two-phase closed thermosyphon ensuring to the readers to be familiar with it, in which the importance of the TPCT and its application scopes were explored. Moreover, the physical concepts of heat transfer and heat transfer mechanisms when using nanofluids were detailly explained and discussed.

It is noticed that inferences reported by different researchers using various analyses are contradictory, further investigations must be performed to fathom the thermophysical behaviour of nanofluids.

In general, nanofluids outperformed the conventional working fluids in perspective of enhancing the TPCT thermal performance to some extent, in which it stills representing a serious challenge due to cost of production and stability issue.

CHAPTER III

Heat Transfer Enhancement in TPCT Using Cellulose Nanofiber: Experimental Study

III.1. Introduction:

From the literature survey in the previous chapter, it was noticed that the mentioned nanofluids are redundantly used in this field. Withal, clustering and sedimentation are a standing issues which pushed scientists to add surfactants and strive to obtain a stable and thermally effective suspensions. Although the good characteristics of cellulose, only three works were conducted using cellulose nanofiber within a TPCT. Therefore, with the aim of enriching the literature, this work represents a detailed process of an experimental investigation performed on a miniature copper two-phase closed thermosyphon using CNF nanofluid, with purpose of figuring out their impact on heat transfer in the TPCT. This chapter explains the steps of the experimental study conducted in this research as follow:

- Choice of nanofluid (advantages and characteristics of CNF).
- Preparation of CNF suspensions.
- Description of the necessary devices and their role.
- The assembly and connection of all devices.
- Launch of the experimental study and data recording.
- Uncertainties of the reduced data.

III.2. Source and characteristics of cellulose nanofibers:

Cellulose is abundant, eco-friendly, biodegradable, biocompatible and non-toxic organic polymer extracted from trees wood. The extraction process is presented briefly in Fig III.1.

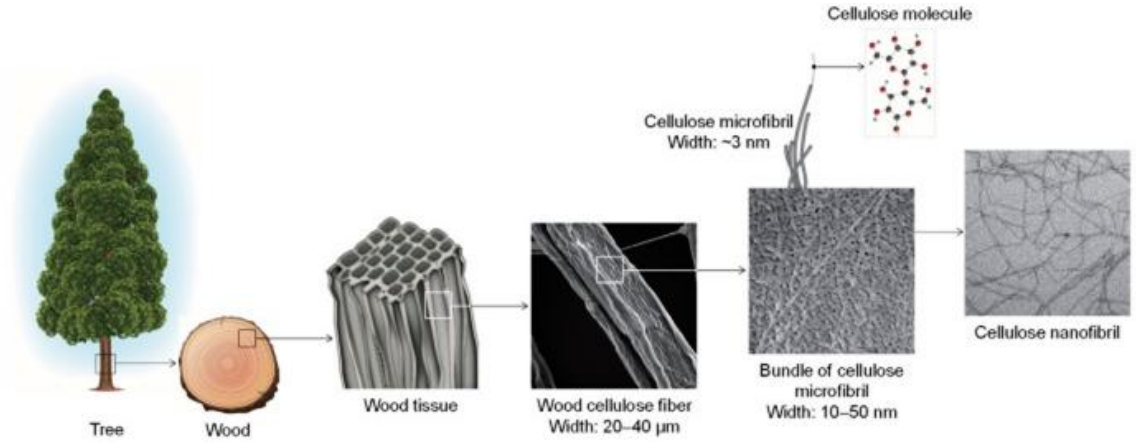

Fig III.1: Process of cellulose nanofiber extraction [77]

III.3. Applications of cellulose nanofibers:

Despite its low thermal conductivity, its feasibility was found to enhance the critical heat flux of water and to maintain dispersed and stable within water due to its low zeta potential [78]. Therefore, Cellulose is implemented in several fields such as cement mixture preparation as it maintains the mixture cohesive [79].Application scopes of Cellulose nanofiber are summarized in Fig III.2.

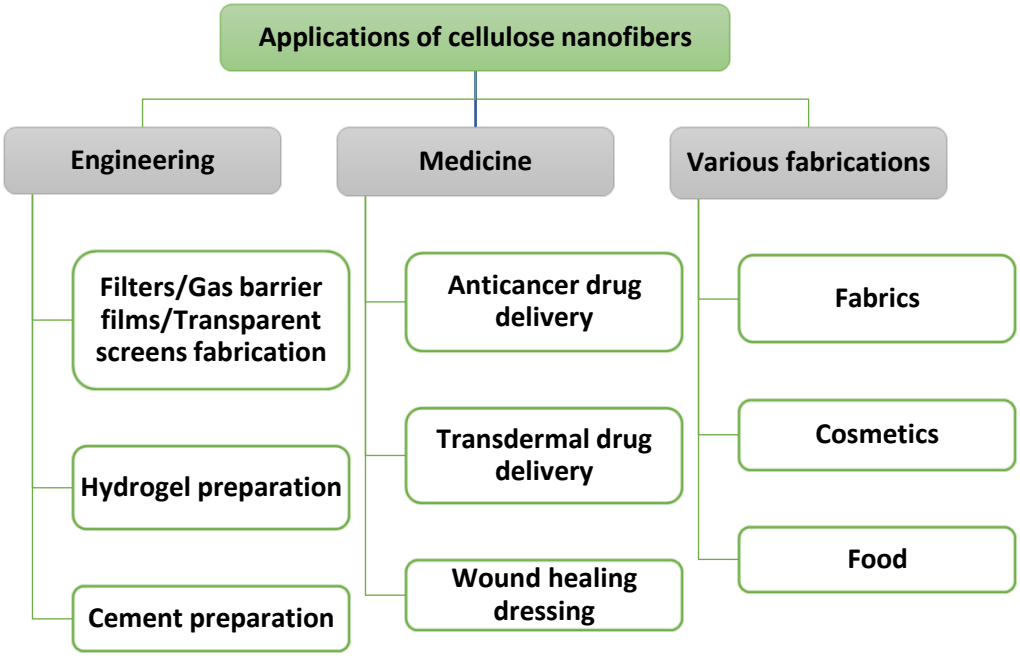

Fig III.2: Application scopes of Cellulose nanofiber

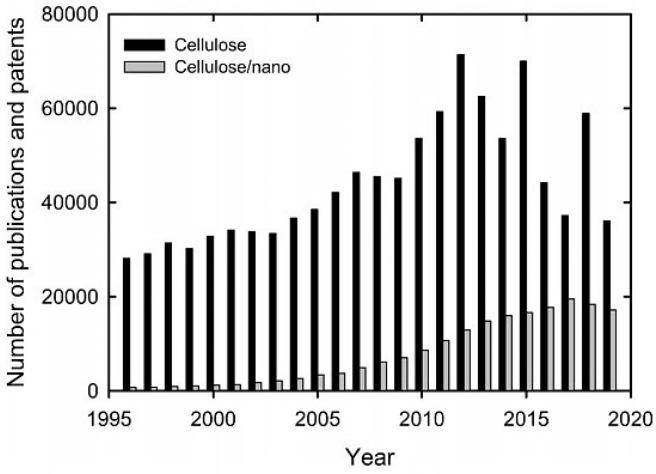

Fig III.3: Annual numbers of publications and patents for the terms “Cellulose” and “Cellulose and Nano” [77]

Due to the diversity of cellulose nanofiber applications, interest of researchers on it raised in the last decades. Annual numbers of publications and patents for the terms “Cellulose” and “Cellulose and Nano” are depicted in Fig III.3.

III.4. Economic insights of cellulose nanofibers in nanoparticles market:

The represented histogram in Fig III.4 is the outcome of reviewing several sources concerning nanomaterials [80,81,82]. It provides the average price of some nanoparticles avalaible in nanoparticles market. Cellulose nanofibers ranked first as the cheapest nanoparticles. Furthermore, it is non-toxic, only allergic reactions may appear in case of eyes contact or inhaling [83].

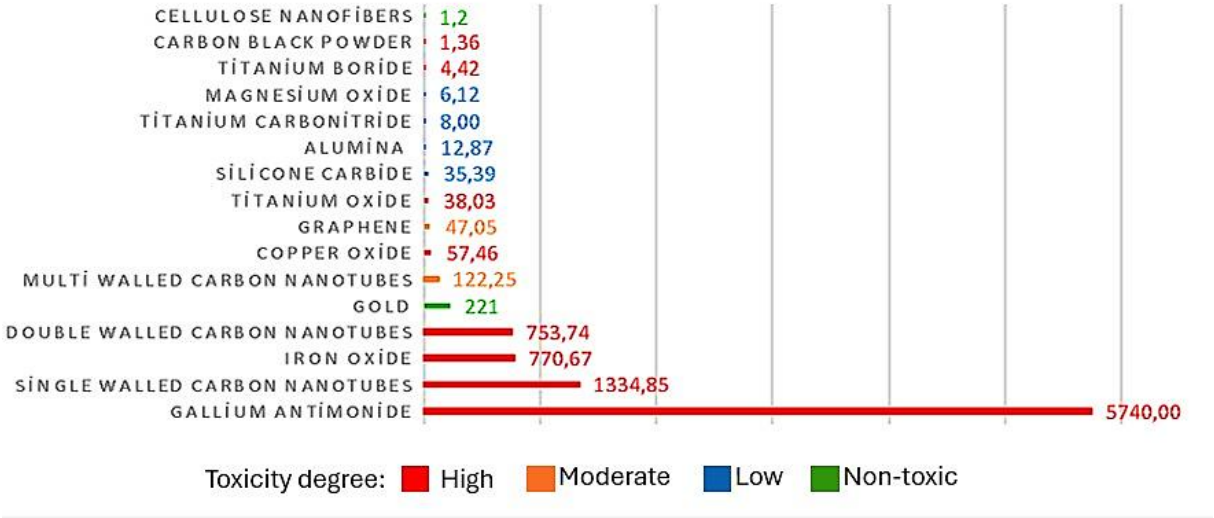

Fig III.4: Average price of nanoparticles with €/g

III.5. Cellulose nanofiber nanofluid preparation:

III.5.1. Characteristics of the purchased cellulose nanofiber:

The CNFs used in this study was purchased from Nanografi company. The following description is token from the DATA sheet furnished by the seller company, (Appendix.1).

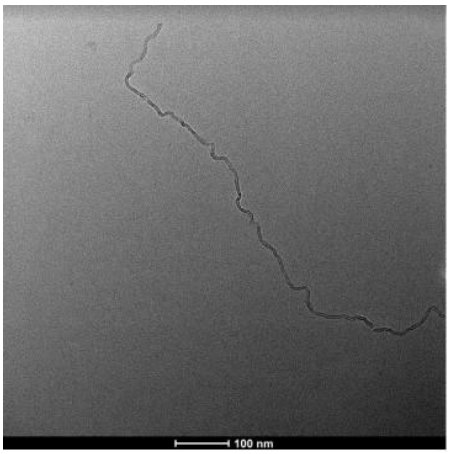

Fig III.5: TEM image of one fiber of cellulose nanofiber used in the current study

Table III.1: Characteristics of the purchased cellulose nanofiber

Appearance (Color)	White
Appearance (Form)	Dry powder (~4 wt.% moisture)
Average Particle Size	Diameter: 10-20 nm, Length: 2-3 µm
Density	1.50 g/cm^3
Melting point	Does not melt
Solubility	Insoluble in water and common organic solvents

III.5.2. Steps of preparation of CNFs nanofluid suspensions:

Three CNF suspensions of 0.5, 1 and 2 vol.% were prepared using two-steps method [84]. Firstly, the suitable weight of CNF powder for each concentration is weighted using an electronic analytical balance (DAIHAN Biomedical), and then the CNF is homogenized with deionized water using a magnetic stirrer (ISOLAB- LABORGERATE GmbH) for 5, 10 and 15 min at 700 rpm for each concentration respectively, followed by an ultrasonic dispersion using ultrasonic bath (HYDRA) for 30 min, Fig III.6. The three prepared CNFs suspensions are shown in Fig III.7.

Fig III.6: Preparation process of cellulose nanofiber nanofluid [87]

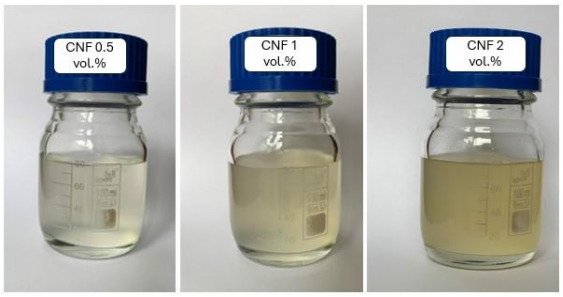

Fig III.7: Prepared CNF suspensions

Mass of CNFs for each concentration is calculated using Percent by volume (vol.%) formula as follow:

$$\Phi = \frac{\text{Volume of solute}}{\text{Volume of solution}} \text{ x } 100 \quad => \quad \text{Volume of solute} = \frac{\Phi \text{ x Volume of solution}}{100} \qquad \text{(III.1)}$$

$$\text{Mass of solute} = \text{Density of solute x Volume solute} \qquad \text{(III.2)}$$

- Density of CNF = 15 g/cm^3
- Volume of solution = 80 ml

Φ = 0.5 Vol.% => Mass of solute CNF = 0.6 g
Φ = 1 Vol.% => Mass of solute CNF = 1.2 g
Φ = 2 Vol.% => Mass of solute CNF = 2.4 g

III.6. Preparation of the experimental stand:

III.6.1. The two-phase closed thermosyphon under study:

The two-phase closed thermosyphon under the study is a copper sealed tube with length of 340 mm. As depicted in Fig III.8, the TPCT is split into three parts with 110 mm of length for both evaporator and adiabatic section, and 120 mm for condenser section. Inner and outer diameter are 10 and 12 mm, respectively. The TPCT is set to the vertical position, and both evaporator and adiabatic sections were thermally insulated using multiple layers of glass wool to eliminate heat loss.

Fig III.8: Two-phase closed thermosyphon under study

III.6.2. Vacuum and filling system:

The TPCT is evacuated using vacuum pump (Value VE 115N), and a mobile system containing vacuum meter (PAKKENS) and extra valve was used to control vacuum pressure before and after filling process with a thin syringe.

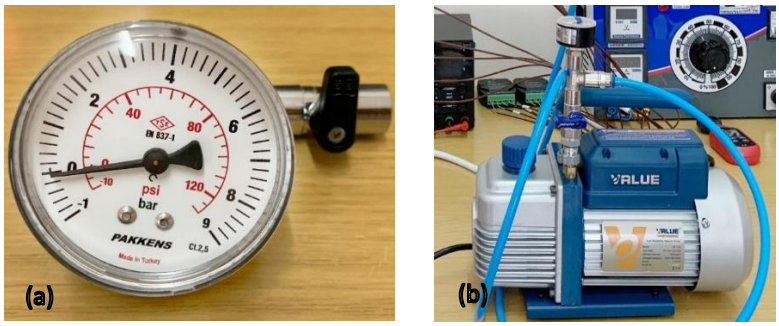

Fig III.9: Vacuum system: (a) Vacuum meter (b) Vacuum pump

III.6.3. Heating system

AC power supply unit (VARSAN). Ground connection and security standards were applied. The evaporator section was heated using a circular sheet resistance leaving a suitable side space to connect thermocouples.

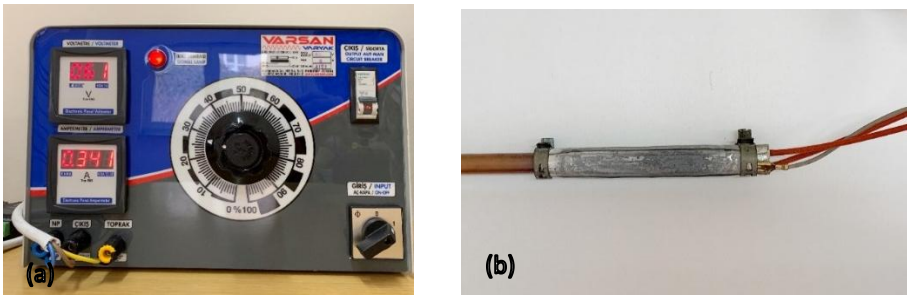

Fig III.10: Heating system: (a) AC power supply unit (b) Sheet resistance covering the evaporator section

III.6.4. Cooling system

Two snail fans were placed facing up to the condenser section, where the blown air was concentred with the help of a rectangular nozzle, with uniform velocity of 8 m/s measured using anemometer (UNI-T UT363).

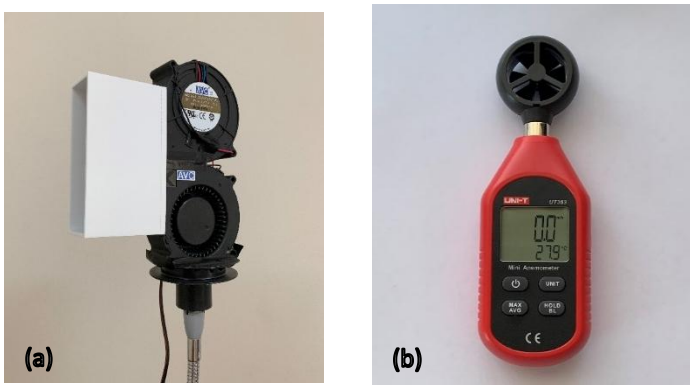

Fig III.11: Cooling system: (a) Snail fans (b) Anemometer

III.6.5. DATA recording system

The wall temperature of the TPCT was measured using ten thermocouples of T types connected to universal data logger (UDL100-ORDEL). Extension wires of each thermocouple are connected using TIG welding to ensure a reliable measurement junction. Furthermore, calibration and reliability control are ensured by the manufacturing company [Appendix.2].

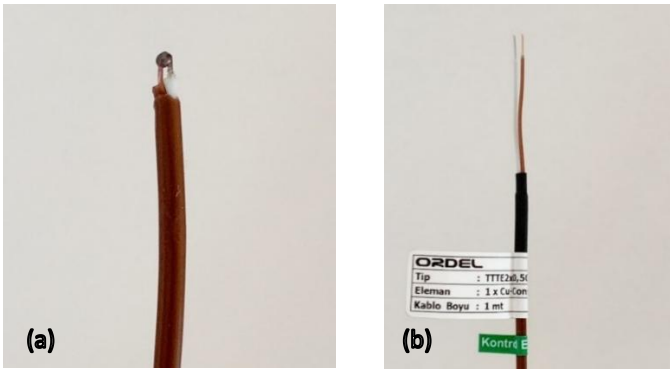

Fig III.12: Thermocouples: (a) Measurement junction (b) Extension wires

Fig III.13: DATA logger

III.7. Experimental process and Data recording:

The apparatus previously described have been assembled to form the experimental stand ready to work. Fig III.14 depicts the assembled experimental apparatus, and every instrument is labelled schematically in Fig III.15 and it is described below.

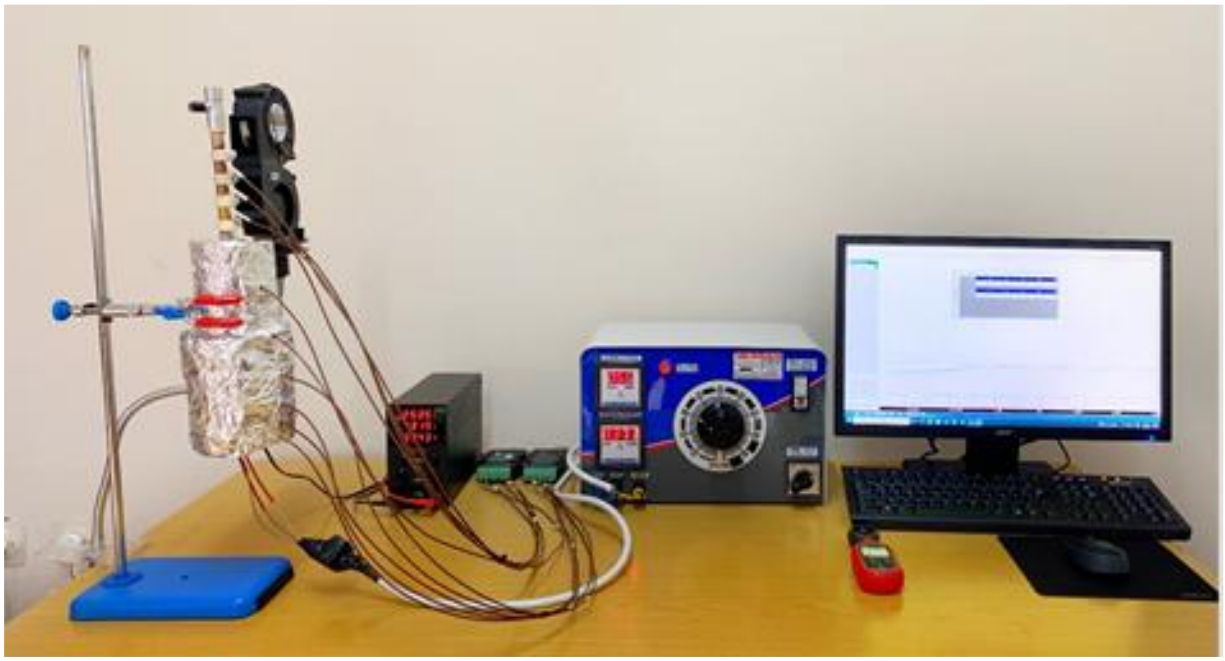

Fig III.14: Experimental apparatus [85]

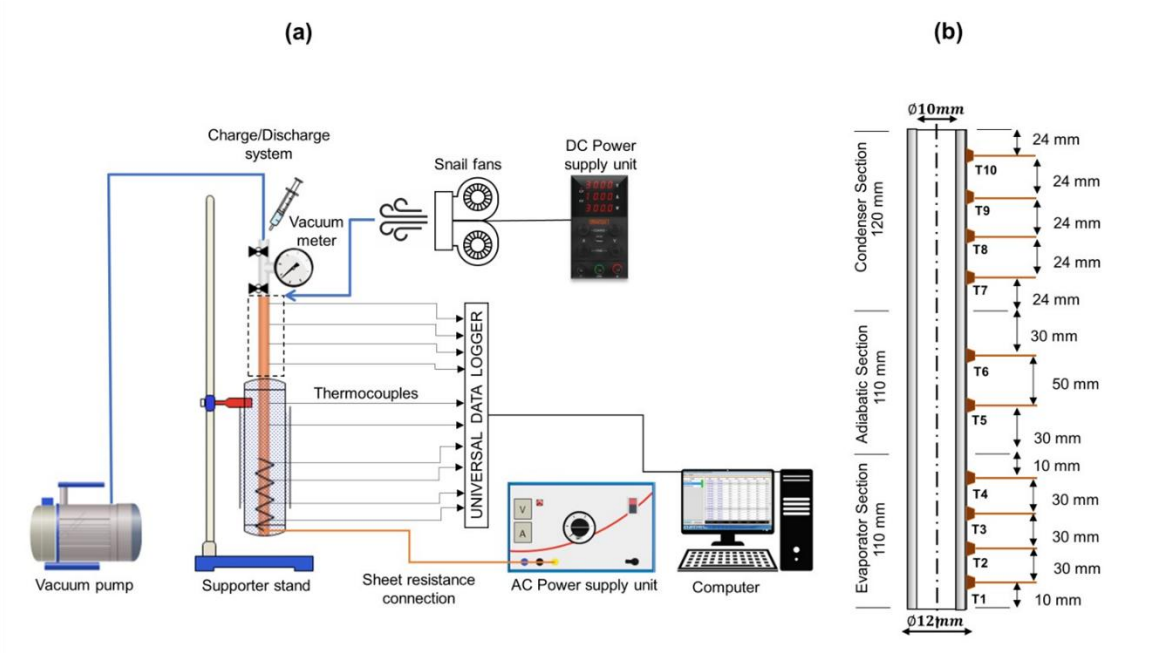

Fig III.15: Comprehensive schematic of experimental apparatus and thermocouples locations (a)Experimental apparatus (b) Technical drawing of the TPCT and location of thermocouples [85]

For each working fluid the experiments are done with three different filling ratios and seven heat loads, which gives totally 84 experiments. Table III.2 summarizes the variables and inputs of the experimental work., and the executed steps to take measurements for each experiment are explained below.

Table III.2: Experimental parameters [85]

	Heat load	**Filling ratio**	**Working fluid**	**Air flow**	**Vacuum pressure**
Values	20,30,40,50, 60,70,80 W	25%,50%,75%	DI CNF 0.5 vol.% CNF 1 vol.% CNF 2 vol.%	8 m/s	0,2 bar

III.7.1. Cleaning of the TPCT:

The first step involves cleaning the TPCT in order to eliminate all impurities found in the internal surface of the tube as these could contaminate the working fluid and therefore disrupt the system performance.

III.7.2. Vacuum of the TPCT:

The non-condensable gases which impede the condensate from return back to the evaporator were evacuated from the TPCT using the vacuum pump, where the vacuum pressure was set at 0.2 bar.

III.7.3. Filling of the TPCT:

After cleaning and evacuation of the TPCT, the working fluid is injected inside carefully with help of syringe and ball valve.

The filling ratios varied to 25, 50 and 75% for each working fluid. the total volume of the evaporator section is calculated using its dimensions (L =110 mm, r =5 mm), and then volumes adequate to each filling ratio are calculated too.

V_e = 8,64 ml

V_{FR1} = 2.16 ml / V_{FR2} = 4.32 ml / V_{FR3} = 6.48 ml

III.7.4. Launch of the experiment:

After being sure that the system is sealed and under vacuum, the heat is applied and controlled from AC power supply unit. Steady state was considered, when wall temperature change with ± 0.1 °C every 5 min.

III.7.5. Data recording:

The transmitted measurements are downloaded from ORDEL software with recording range of 10 seconds.

III.8. Data reduction and uncertainties

The random errors of experiments were reduced by repeating the measurements three times and taking the arithmetic mean value. While systematic errors were reduced using the formulas below.

Q_{in} is the heat load applied on the evaporator section, and it is obtained from equation (III.3) where V is voltage, and I is current.

$$Q_{in} = V.I \quad \text{(III.3)}$$

The total thermal resistance of the TPCT was calculated using equation (III.4).

$$R_{tot} = \frac{\bar{T}_e - \bar{T}_c}{Q_{in}} \quad \text{(III.4)}$$

Both boiling and condensation heat transfer coefficients are calculated using the following equations respectively:

$$\text{BHTC} = \frac{Q_{in}}{A_{e,i}(\bar{T}_e - T_v)} \quad \text{(III.5)}$$

$$\text{CHTC} = \frac{Q_{in}}{A_{c,i}(T_v - \bar{T}_c)} \quad \text{(III.6)}$$

Thermal efficiency η of thermosyphon is defined as the cooling capacity of the system. In other word, it is the ratio of removed heat quantity at the condenser section to the loaded heat quantity at the evaporator section.

$$\eta = \frac{Q_{out}}{Q_{in}} * 100 \quad \text{(III.7)}$$

Q_{out} was calculated using the external heat transfer coefficient h_o of the condenser section, which was obtained using Nusselt correlation for cross flow over a cylinder (III.10), [86].

$$Q_{out} = h_o . A_{c,o}(\bar{T}_c - T_\infty) \quad \text{(III.8)}$$

$$h_o = \frac{Nu \cdot k}{L_c} \quad \text{(III.9)}$$

Nusselt number is calculated using the following correlation for flow cross a cylinder for: Re.Pr>0.2.

$$Nu = 0.3 + \frac{0{,}62.Re^{\frac{1}{2}}.Pr^{\frac{1}{3}}}{\left[1+\left(\frac{0.4}{Pr}\right)^{\frac{2}{3}}\right]^{\frac{1}{4}}} \times \left[1 + \left(\frac{Re}{282000}\right)^{\frac{5}{8}}\right]^{\frac{4}{5}} \quad \text{(III.10)}$$

Reynolds and Prandlt number are calculated using equation (III.11) and (III.12), respectively

$$Re = \frac{\rho V L_c}{\mu} \quad \text{(III.11)}$$

$$\Pr = \frac{\mu Cp}{k} \quad \text{(III.12)}$$

Both, Re et Pr are calculated using air characteristics at film temperature T_f.

$$T_f = \frac{\bar{T}_c + T_\infty}{2} \quad \text{(III.13)}$$

Uncertainties of the obtained results from previous equations are calculated using Kline & McClintock formula (III.14), [87]. Uncertainties of all parameters are given in Table III.3 below.

$$\delta R = \left[\sum_{i=1}^{n} \left(\frac{\partial R}{\partial xi}\partial x_i\right)^2\right]^{1/2} \quad \text{(III.14)}$$

Table III.3: Uncertainty of measurements and parameters

Measurements	**Uncertainty**
Wall temperature (T- type thermocouple ORDEL)	± 0.1 °C
Cooling air velocity (Anemometer Unit-365)	± 1 m/s
Heat load (AC power supply unit VARSAN)	1.69%
Parameters	
Heat transfer coefficients [W/m^{2}K]	10.14%
Thermal efficiency [%]	9.32%
Total thermal resistance [K/W]	1.71%

III.9. Conclusion:

This chapter broached all experimental steps of this work, explaining devices role and applied experiments. It allows also the readers to understand the conducted study with all necessary information, which is helpful for beginner researchers to refer to it for similar studies. Results of this work are compiled and discussed in the next chapter.

CHAPTER IV

Results and Discussion

IV.1. Introduction

This chapter depicts and analyses the results of the experimental study, which was explained in the previous chapter. The wall temperature distribution of TPCT and its total thermal resistance are the mirror of the thermal performance of the device. From literature survey, it was noticed that scientists opt for reducing all of the evaporator wall temperature, the temperature difference between two ends and the total thermal resistance.

Relying on this, the effects of filling ratio and cellulose nanofiber nanofluid on wall temperature distribution, total thermal resistance and the startup of the TPCT under study are analysed, compared and discussed. Additionally, only for the high and low extremity results, the transient wall temperature distribution is analysed. Beside this, the boiling and condensation heat transfer coefficients and efficiency are analysed too.

IV.2. Impact of CNF and filling ratio on the wall temperature distribution:

The wall temperature distribution of the TPCT at steady state for all experimental cases is shown in Fig IV.1. Generally, with rise of heat load, the average wall temperature of the TPCT increases, while the temperature difference between its two ends (T_1 and T_{10}) decreases. All temperature distributions have similar profiles, and no dry out was remarked in any case.

It is obviously observed that the highest evaporator wall temperature and the largest temperature difference between the evaporator and the condenser manifest when using DI as working fluid with FR of 75% at all heat loads. While the lowest ones manifest with CNF 1 vol. % at FR 75%.

All of CNF concentration, filling ratio and heat load have an apparent impact on the wall temperature distribution along the TPCT, but the optimum CNF concentration varies with change of FR and heat load, and similarly for the optimum FR that changes according to CNF concentration and heat load. This deduction agrees with findings of Gallego et al [54]. In which, decreasing FR of DI reduced the evaporator wall temperature by 28.29% and 34.09% for FR 50% and FR 25% respectively compared to FR 75% at 20 W. This reduction ratio decreases with increasing heat load to 19% and 20.68% at 80 W, respectively. Furthermore, using CNF suspensions reduced the evaporator wall temperature, especially for high FR to reach a reduction of 40% with CNF 1 vol. % with FR 75% compared to DI with FR75% at 20 W, and at 80W the reduction was found to be 23%. It is remarked that impact of CNF is intense at low

heat loads, and the average evaporator wall temperature for all concentrations tend to converge with rising heat load.

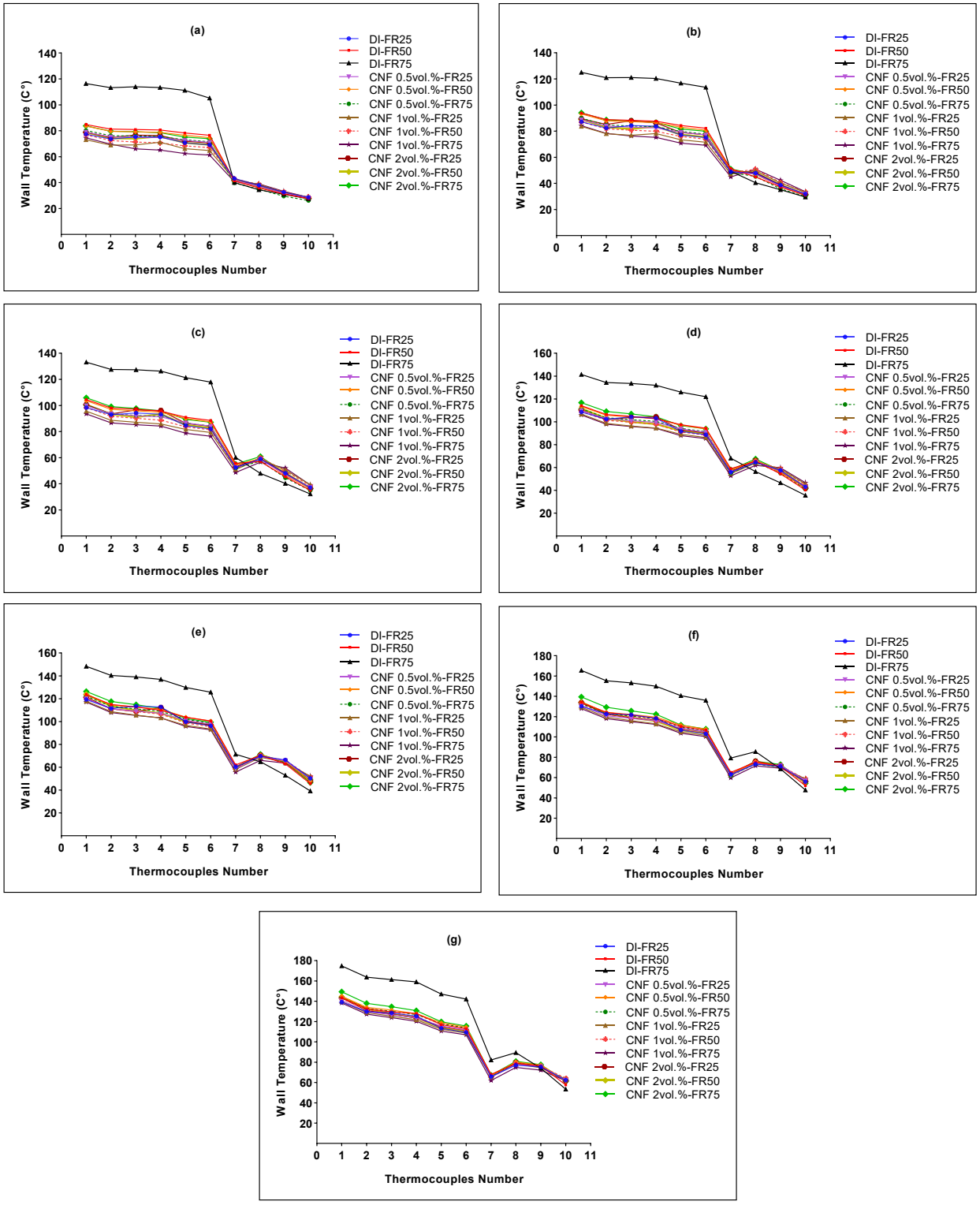

Fig IV.1: Wall temperature distribution along the heat pipe for all working fluids at various heat loads. (a)20 W, (b) 30 W, (c) 40 W, (d) 50 W, (E) 60 W, (f) 70 W, (g) 80 W [85]

The average condenser wall temperature also increases with rise of heat load. The condenser wall temperatures of all cases are uneven but very near to each other, except the one of DI with FR 75% which owns the lowest condenser temperature, and this implies that less heat is extracted from the evaporator with it. With increasing heat load, T_8 and T_9 increased and became equal to each other and bigger than T_7 and T_{10}, so it gave a convex curve to the temperature profile of the condenser part for all cases, except DI with FR75% which keeps a descendant shape till 70 W and 80 W where T_8 becomes higher than T_7. This warping of temperature profile is due to the sudden temperature drop of the vapor in the entry of the condenser at T_7, and presence of a cold end at T_{10}, this can be explained by the existence of non-condensable gases inside the TPCT. These non-condensable gases can come from the filling process which is not 100% efficacious. As they have a lower density, they cluster in the upper end of the TPCT, and inhibit the vapor from reaching there, resulting in lower temperature at T_{10}. Therefore, the efficient heat sink happens at the region surrounding T_8 and T_9.

IV.3. Impact of CNF and filling ratio on the total thermal resistance

The total thermal resistance of the TPCT decreases for each case with rise of heat load as shown in Fig IV.2. When using DI, decreasing the FR leads to decrease the thermal resistance by 40.85% and 51% for FR 50% and FR 25%, respectively compared to FR 75% at 20 W. FR has a remarkable impact on R_{tot} when using DI. While when using CNF, FR impact diminishes. The most significant decrease in R_{tot} occurred when using CNF 1 vol. % with FR 75%. This decrease was by 58.78% and 33.65% for 20 and 80 W respectively compared to DI with FR 75%. Whereas, using CNF with 2 vol. % dramatically re-increased the R_{tot}.

The thermal resistance is a result of vapor bubbles accumulation at the solid-liquid interface on the inner wall of the evaporator, which impedes the heat transfer from the solid to the liquid, when the evaporator filling ratio increases, the vapor bubbles amount rises and lead to a higher thermal resistance of the evaporator, but the presence of nanoparticles within the liquid provides nucleation sites and helps bombarding the vapor bubbles and reduce that thermal resistance [88]. It can be concluded that the evaporator thermal resistance dominates the total thermal resistance.

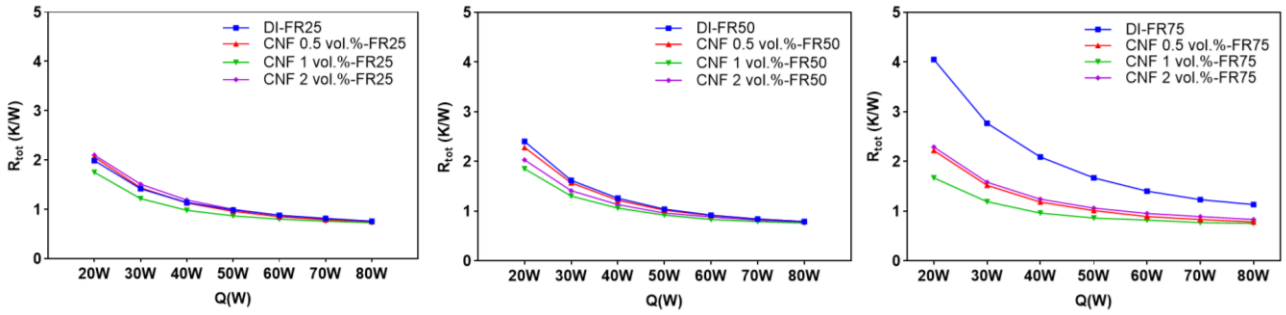

Fig IV.2: Total thermal resistance of the TPCT for all working fluids with different filling ratios at various heat loads [85]

Indeed, wall temperature distribution of the TPCT is a mirror of its total thermal resistance, in which the highest evaporator wall temperature and the largest temperature difference between the two ends of the device reflect the highest thermal resistance, such in case of DI FR 75%. Similarly, the lowest evaporator wall temperature and the smallest temperature difference between the two ends of the device reflect the lowest thermal resistance, such in case of CNF 1 vol. % FR 75%. As shown in Fig IV.1 with increasing heat load the temperature difference between two ends of the TPCT decreases which is reflected on the total thermal resistance decrement.

IV.4. Impact of CNF nanofluid and filling ratio on the TPCT startup

The startup of the TPCT is defined as the transient process from initial status to the steady status of the device operation. In other word, it is the period taken to the circulation of vapor and liquid flux for once, from applying heat load and vapor departure toward the condenser to the return of condensate to the liquid pool.

The startup is characterized by its duration and temperature, and it is altered by many working conditions. In Fig IV.3 the time and the temperature of each startup for all working fluids with different FR at 20 W is depicted. Impact of FR on the startup is intense when using DI, while CNF concentration has a stronger influence at all filling ratios. The longest startup manifests with DI with FR 75%, where it lasted about 900 s and wall temperature reached 120 °C at the bottom. Unlike, the shortest startup manifests with CNF 1 vol. % with FR 75%, and it lasted about 600 s with a temperature less than 70 °C. The maximum reduction in startup time and temperature is noticed between those cases. In which, the startup time shortened by 33%

and wall temperature at the bottom decreased by 42%. Whereas, increasing CNF concentration to 2 vol. % deteriorated the startup regarding to CNF with 1 vol. %.

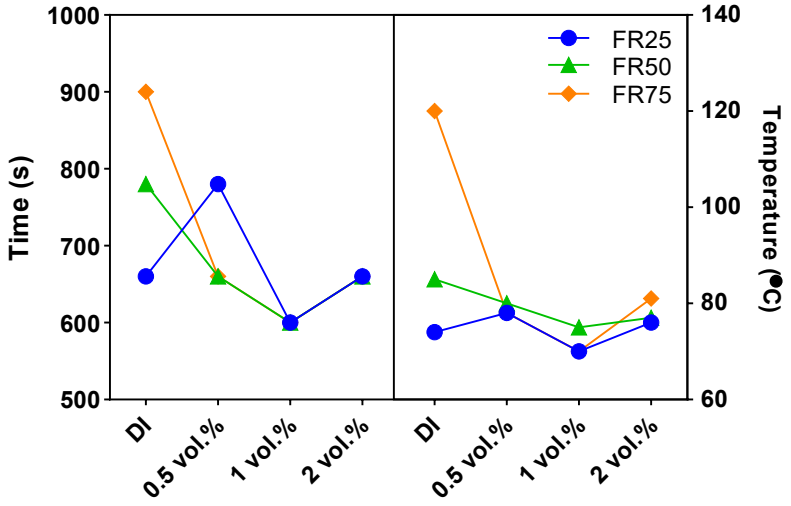

Fig IV.3: Duration and temperature of the startup for all working fluids with different filling ratios [85]

IV.5. Analysis of transient wall temperature for cases of highest and lowest wall temperature distribution:

The TPCT is made from opaque material which inhibit visualization of boiling, evaporation and condensation regimes. Thus, some studies relied on numerical models to predict the phase change process, or experimentally by using glass TPCT to observe it [52,89]. Else way, wall temperature variation through time can also help to figure out what happens inside the TPCT. In this section, transient wall temperature variation at all thermocouples locations from the minimum to the maximum applied heat load is analysed. Only the cases of highest and lowest wall temperature distribution are considered for this analysis which are DI with FR 75% and CNF 1 vol. % with FR 75%, as depicted in Fig IV.4 (a, b) respectively.

The wall temperature of the TPCT increased gradually with application of initial heat load of 20 W to the evaporator. The first transient phase before reaching the steady state is called startup as defined in the previous section. Thereafter, higher heat loads were applied successively. Here, for both cases, no sudden rise of evaporator wall temperature was noticed, which implies that the TPCT operates normally without any dry out.

In case of using DI with FR 75%, the rise of evaporator wall temperature after applying 70 W was severe comparing to the other experiments, and followed by an intense oscillations at

T_4 for 80 W. At the condenser section, obvious oscillations started after applying 40 W, especially with T_7, due to the increase of the vapor mass achieving the condenser with heat load rise. After applying 70 W, a sudden intense oscillations occurred with T_8 till it crossed and passed T_7 at point A, Fig IV.4 (a). Frequency of these oscillations lightened at 80 W, while its amplitude expanded. Wavering of temperature was noticed also at the adiabatic section, which implies that there is a change in boiling regime and vapor flow pattern, and this is explained by the oscillation of T_4 which is located at the upper level of liquid pool. Consequently, a change in condensate flow pattern occurred. In other word, flow instability occurred after applying 70 W.

When using CNF 1 vol. % with FR 75%, slight fluctuations occurred at all evaporator section. After applying the initial heat load of 20 W, the condenser wall temperature rises quickly accompanied with oscillations. At point A, Fig IV.4 (b), T_8 crossed and passed T_7 immediately after applying 30 W. Also, T_9 crossed and passed T_7 after applying 40 W at point B. Thereafter, T_7 and T_{10} became equal and lower than T_8 and T_9 at 80 W, and that is reflected in the convex curve of the condenser wall temperature in Fig IV.1 (g). Contrary to the case of DI with FR 75%, any flow instability did not occur at high heat loads. This result is consistent with Lee et al. [66] inference that CNF contribute to stabilize the device operation process.

These overshoots of temperature in the condenser section happens twice with CNF 1.vol% and earlier than the case of DI, which implies that an important amount of vapor reaches the condenser quickly and leads to better heat sink and lower evaporator wall temperature. Moreover, when applying 20 W to the TPCT, the temperature of adiabatic section T_6 is obviously lower than T_5 when using DI, and quasi equal when using CNF 1.vol%, which proves that vapor is released with CNF 1.vol% quicker than with DI. This inference is already proven in the precedent section and framed on Fig IV.4 (a, b), that using CNF 1.vol% shortened the startup time by 33%, and its temperature also.

Analysis of wall temperature variation over time at all thermocouples location contributed to figure out that the TPCT functioned normally, without any dry out, also the effect of CNF on the startup and the transient wall temperature was noticed, but it still obscure to know what happens exactly inside, as boiling and condensation regimes evolution.

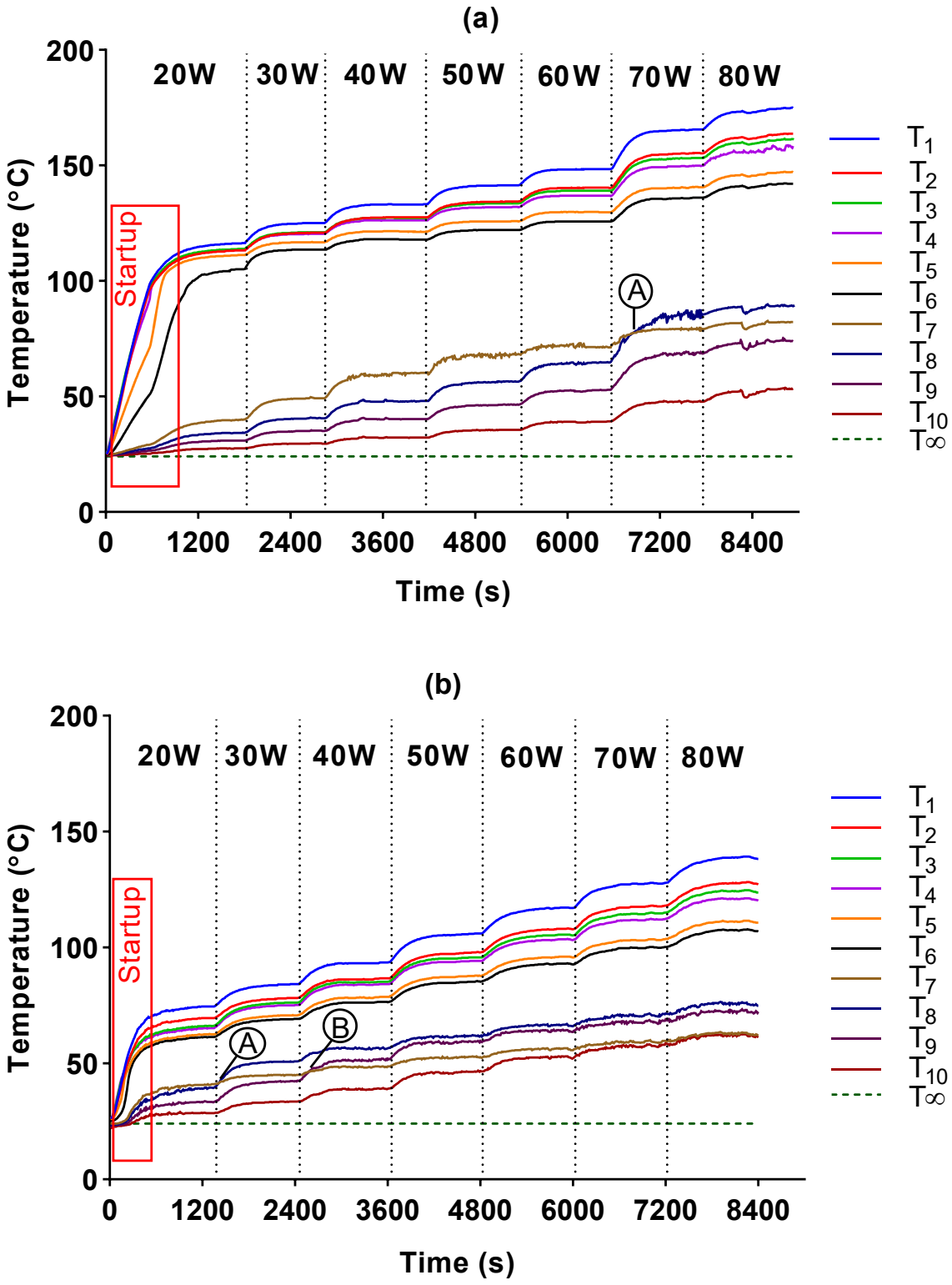

Fig IV.4: Wall temperature variation through time at all thermocouples location from the minimum to the maximum applied heat load. (a) DI with FR 75%, (b) CNF 1 vol. % with FR 75% [85]

.

IV.6. Boiling and condensation heat transfer coefficients:

The boiling heat transfer coefficient is affected by both of filling ratio and working fluid as shown in Fig IV.5, and it changes randomly with increasing heat load, giving a fluctuated graph lines. Comparing to DI, adding CNF with 0.5, 1 and 2 vol. % with FR 25% at 20 W ameliorated the BHTC by 30.91%, 5.88% and 0.47% respectively. While at 80 W the improvement reached only to 17.07%, 5.59% and 7,79%, respectively. Contrary, with FR 50%,adding CNF deteriorated the BHTC by 3.72%, 11.71% and 20.96%, respectively at 20 W. At 80 W, for CNF 0.5 vol.%, small amelioration occurred about 3,51% while adding CNF with 1 vol.% and 2 vol.% deteriorated it again by 2.51% and 8.22% respectively. Similar point is noticed with FR 75%. At the case of DI with FR75%, a sudden decrease in BHTC at 70W and 80W was remarked. Ghanbarpour et al [90], referred these fluctuations to the change in the inner evaporator surface caused by nanoparticles. But in this study, even with deionized water at different filling ratio a random tendance of the BHTC manifested with increasing heat load, and that may be due to the change in boiling regime. However, the highest BHTC manifests when using CNF with 0,5 Vol.% at FR 25% at all heat loads.

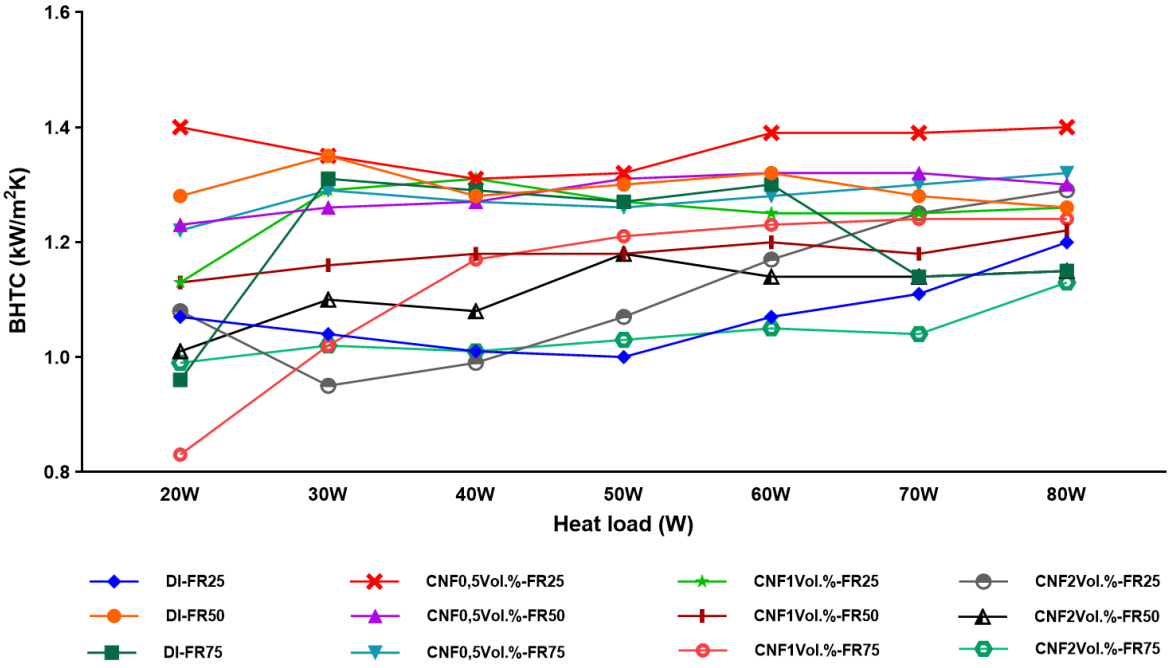

Fig IV.5: Boiling heat transfer coefficients

As shown in Fig IV.6, CHTC increased linearly with heat load rise, because rising the applied heat intensifies the boiling and results larger amount of vapor upward, thus higher heat transfer occurs in condenser section. CHTC varies also with change of filling ratio and CNF concentration. FR 25% showed better CHTC when using DI or CNF 0.5 vol.%. On the contrary, when using higher concentrations, FR 75% and FR 50% showed better CHTC with CNF 1 vol.% and CNF 2 vol.% respectively. Adding CNF with 1 vol.% with FR 75% improved the CHTC up to 183% at 20 W and 30 W compared to DI with the same filling ratio.

Since vapor and liquid move in counter directions, a shear force occurs between liquid-vapor interface, which entrains liquid droplets into the vapor moving towards the condenser. Some studies mentioned that nanoparticles do not affect the condenser heat transfer because small and negligible quantity of nanoparticles reaches the condenser and do not deposit there [91,92,93]. In this study, the condenser wall temperature and CHTC are affected by heat load, filling ratio and CNF concentration as well. Nanoparticles influence the condenser section indirectly, because their presence changes the boiling regime and the generated vapor mass, also the latent heat of vaporization of base fluid [94]. Thus, it alters the condensation film thickness, CHTC and wall temperature [95,96].

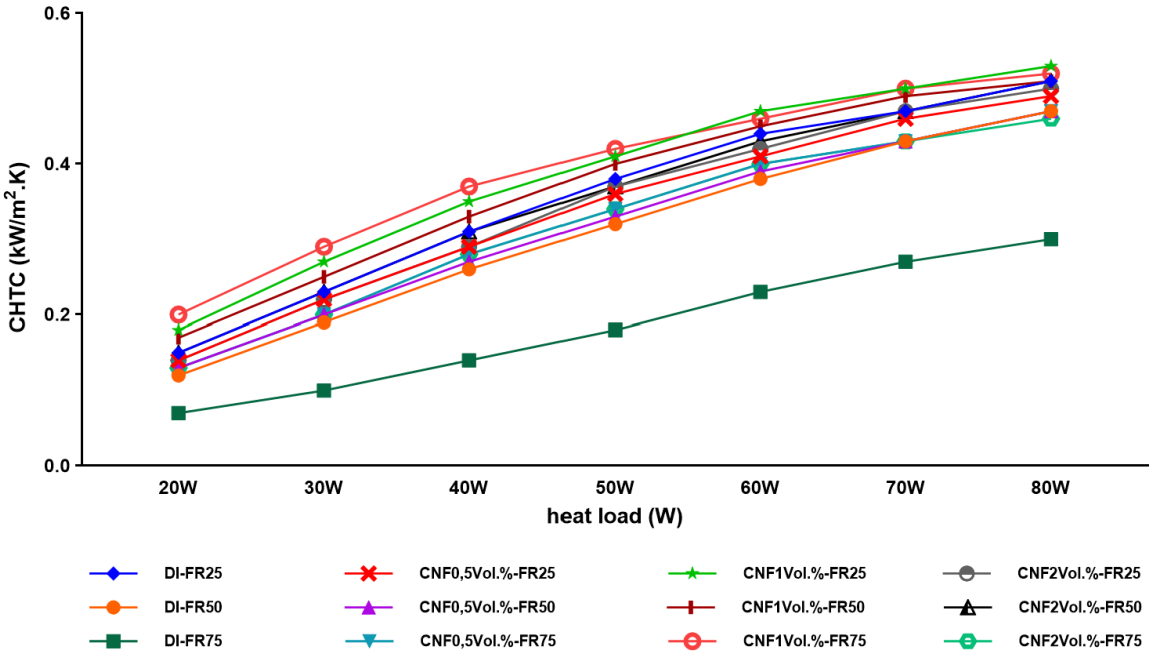

Fig IV.6: Condensation heat transfer coefficients

IV.7. Thermal efficiency of the TPCT:

Fig IV.7 depicts the thermal efficiency of the TPCT for all cases, which was obtained using equation (5) . At low FR, adding CNF with 0.5 vol.% led to a small deterioration in the thermal efficiency. But increasing CNF concentration enhanced it. Where the best thermal efficiency was found when adding CNF with 1 vol.% and FR 50% from 20W to 60W. Generally, the thermal efficiency of the TPCT tends to increase with rising heat load and then decrease, except in case of DI with FR 75%, in which a sudden improvement was noticed at 70W.

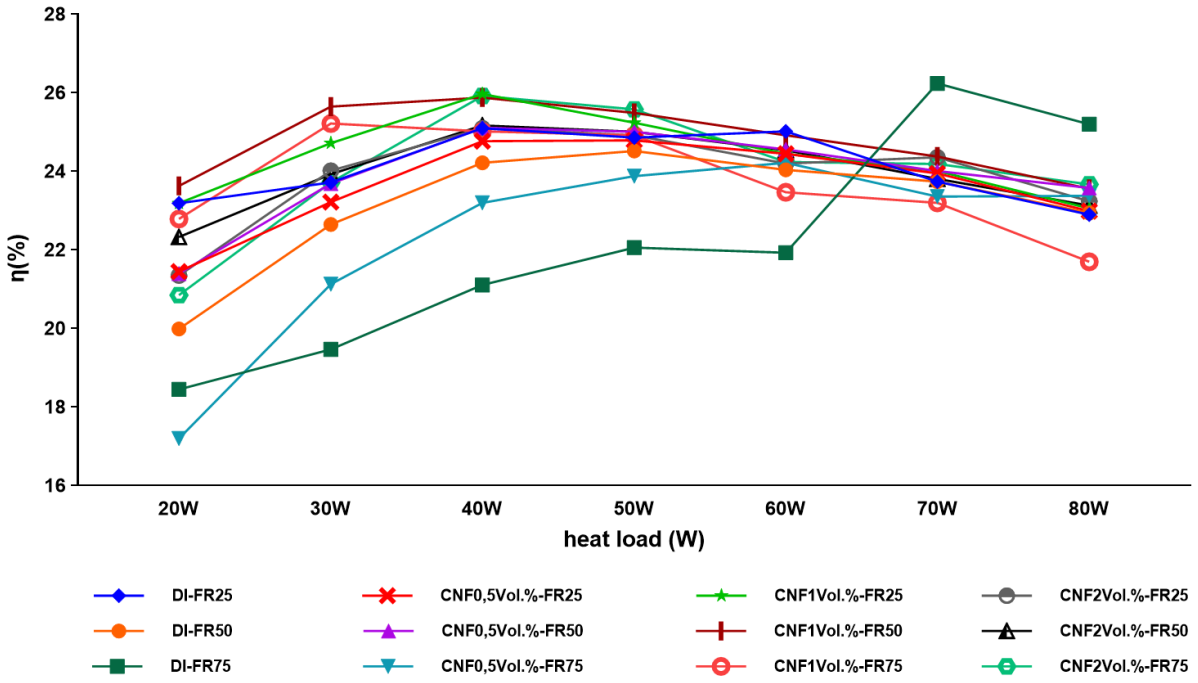

Fig IV.7: Thermal efficiency of the TPCT

IV.8. Discussion of impact of nanofluids on heat transfer:

Indeed, due to its Brownian motion, CNF intensifies the turbulence and boiling and provides nucleation sites and helps bombarding the vapor bubbles that form the boiling film on the inner wall of the evaporator. Furthermore, bubbles bursting results both larger number and smaller size of vapor bubbles and provokes their departure from the inner wall quickly, as visualized in wire pool boiling experience conducted with CNF suspension conducted by Choi et al. [60] and Hwang et al. [78] and that explains the slight fluctuations of evaporator wall temperature (Fig IV.7 (b)), [43]. Thus, the startup accelerates and significant decrease in thermal

resistance occurs. Additionally, even with a stable suspension, nanoparticles presence changes the wall surface roughness. In which, an amount of nanoparticles forms a thin porous layer on the inner wall of the evaporator and that leads to change the surface tension and wettability [97, 98]. Consequently, it alters the startup and the whole heat transfer process, as Ma et al. [99] proved that inner surface characteristics have an impact on the thermosyphon startup.

IV.8.1. Impact of nanofluid viscosity on heat transfer:

The viscosity is a crucial aspect in heat transfer in nanofluids. Although its importance, the impact of nanofluids viscosity has not gained a considerable attention as the other thermophysical properties of nanofluids. Thus, this section focuses on discussing the viscosity role in heat transfer enhancement in nanofluids within TPCT.

Similarly to the other thermophysical properties of nanofluids, viscosity is affected by temperature, nanoparticles characteristics (Shape, size, concentration), shear rates, additives and dispersion technique [100].

Results reported by different studies agree that viscosity increases with increasing concentration of nanoparticles. In other word, nanoclusters formation or clustering in nanofluid typically occured at high nanoparticles concentrations, where van der Waals forces cause agglomeration due to extremely tiny interparticle distances.

Increasing temperature engenders agitation of molecules of base fluid, which intensifies the Brownian motion of nanoparticles. Thus, they move quicker, and interact for shorter time, which leads to break van der Waals forces and reduce the internal frictions and consequently decreasing nanoclusters size and number and gives a lower viscosity. With low concentration, nanofluids behave as a Newtonian fluid, while with high concentration, nanofluids behave as a non-Newtonian fluid [101, 102]. Additionally, the increase in viscosity offsets the increase of thermal conductivity, because nanoclusters and aggregation tend to sediment due to gravity force, which increases the thermal resistance and deteriorates the heat transfer rate [50].

For this reasons, high viscosity was outlined as a non-favourable property for the good operation of the TPCT. But that doesn’t invalidate its potential to enhance the heat transfer to some extent.

Determining the viscosity of a nanofluids can significantly impact the accuracy of numerical analysis of thermal and fluid dynamics for heat transfer and phase change phenomena in TPCT and heat pipes in general. Hence, some correlations were developed to predict the viscosity of

nanofluids, but a correlation for determining the viscosity of nanofibers nanofluid is not developed yet [103].

IV.9. Conclusion

This experimental work studied the impact of filling ratio and cellulose nanofiber concentration on the thermal performance of miniature two-phase closed thermosyphon at various heat loads. Conclusively, the main findings of this work are summarized as follows:

- Filling ratio, CNF concentration, and heat load have a significant impact on the thermal performances of the TPCT. Moreover, there is a trade-off between these parameters, in which the optimum FR changes with variation of both CNF concentration and heat load, and similarly for the optimum CNF concentration that also changes according to FR and heat load.

- The highest evaporator wall temperature and total thermal resistance manifest themselves when using deionized water as a working fluid with FR of 75% at all heat loads, while the lowest ones manifest when using 1 vol.% CNF with FR of 75%. In which, 1 vol.% CNF with FR of 75% reduced the evaporator wall temperature and the total thermal resistance by 58.78% and 40%, respectively, at 20 W compared to DI with FR of 75%.

- CNF with 1 vol.% concentration at FR of 75% accelerated the startup process by 33% of time and 42% of temperature compared to DI with FR of 75%, giving a better thermal performance represented in the lowest thermal resistance and evaporator wall temperature as mentioned above.

- CNF pushed away the occurrence of flow instability at high heat loads. Finally, despite its low thermal conductivity, the organic cellulose nanofiber nanofluids outperformed the deionized water as a working fluid for a miniature two-phase closed thermosyphon. Its positive impact on the device performance is limited by its concentration and other conflicting parameters such as filling ratio.

Design should take these points in consideration; otherwise, deterioration in the thermal performance could manifest. Further works that combine between wall temperature distribution variation and inner changes visualization are strongly recommended to help in analysing the phase change phenomena from reading the wall temperature variation through time.

General Conclusion
And
Perspectives

This thesis broached a general view on heat pipes and the concept of involving nanofluids within to improve their thermal performance. Afterward, a literature survey focused on the Two-phase closed thermosyphon was conducted with aim of understanding the physical concepts of heat transfer and its mechanisms when using nanofluids.

In general, nanofluids outperformed the conventional working fluids in perspective of enhancing the TPCT thermal performance to some extent, in which it stills representing a serious challenge due to cost of production and stability issue. Therefore, the current study came to contribute to investigate the impact of a nanofluid which is non-redundantly used before. This last one is cellulose nanofiber nanofluid based deionized water. After explaining the experimental steps in the third chapter, the fourth one came with important findings that enriches the literature background in heat pipes and nanofluids fields.

Thesis main contributions by order are :

- After a deep research, heat transfer mechanisms within TPCT using nanofluids were deduced and classified.
- The detailed explanation of the experimental study provides an experimental brochure which is helpful for researchers to refer to it for similar studies.
- The selection of cellulose nanofiber nanofluid allowed to obtain valuable results which are not available in literature. Such as the impact of cellulose nanofiber nanofluid on the startup of a miniature two-phase closed thermosyphon.
- Besides, filling ratio and temperature, the impact of cellulose nanofiber nanofluid on a miniature two-phase closed thermosyphon was investigated.
- Finally, the eco-friendly cellulose nanofiber nanofluid succeed to improve heat transfer in a miniature two-phase closed thermosyphon. Yield, its positive impact is limited by its concentration and other conflicting parameters such as filling ratio and temperature.

Perspectives

The results obtained by this study are noteworthy and encourage to pursue this research path. Further directions need to be investigated:

- Providing a study that combines between wall temperature distribution variation and inner changes visualization is strongly recommended to help analysing the phase change phenomena from reading the wall temperature variation through time.
- Creating a User Defined Function (UDF) for Computational Fluid Dynamics (CFD) simulation using two-phase models, with aim to predict flow patterns within the TPCT.

- Adoption of Artificial Neural Networks to predict thermophysical properties of nanofluids, with drawback of correlations for fiber shape nanoparticles. As well as the heat transfer coefficients.

References

[1] D.A.Reay, “The perkins tube-a noteworthy contribution to heat exchanger technology, Heat Recorery Systems” Vol. 2. No. 2, pp. 173-187 (1982)

[2] D. A. Reay *et al.*, “Heat Pipes Theory, Design and Applications Sixth Edition,” 2014. [Online]. Available: http://store.elsevier.com/

[3] Bahman Zohuri ,“Heat Pipe Design and Technology” Modern Applications for Practical Thermal Management. Second Edition. DOI 10.1007/978-3-319-29841-2

[4] A. Faghri, “HEAT PIPES: REVIEW, OPPORTUNITIES AND CHALLENGES,” *Frontiers in Heat Pipes*, vol. 5, no. 1, Apr. 2014, doi: 10.5098/fhp.5.1.

[5] H. Jouhara, N. Khordehgah, S. Almahmoud, B. Delpech, A. Chauhan, and S. A. Tassou, “Waste heat recovery technologies and applications,” Jun. 01, 2018, *Elsevier Ltd*. doi: 10.1016/j.tsep.2018.04.017.

[6] S. Du and Z. Ye, “Analysis and Applications of the Two Phases Closed Thermosyphon Technology in the Highways in Permafrost Regions: A Review,” May 01, 2024, *Multidisciplinary Digital Publishing Institute (MDPI)*. doi: 10.3390/app14104185.

[7] C. Tarau, W. G. Anderson, and C. J. Peters, “Thermal Management System for Long-Lived Venus Landers Acronyms ASRG Advanced Stirling Radioisotope Generator BOM Beginning of Mission BON beginning of normal operation BOP beginning of pre-cooling”.

[8] L Mottet, T Coquard, M. Prat, Heat and mass transfer in the porous wick of a capillary evaporator, ICPM5, 2014.

[9] R. Khodami, A. Abbas Nejad, and M. R. Ali Khabbaz, “Experimental investigation of energy and exergy efficiency of a pulsating heat pipe for chimney heat recovery,” *Sustainable Energy Technologies and Assessments*, vol. 16, pp. 11–17, Aug. 2016, doi: 10.1016/j.seta.2016.04.002.

[10] A. Faghri and Y. Zhang, “INTRODUCTION TO TRANSPORT PHENOMENA,” in *Transport Phenomena in Multiphase Systems*, Elsevier, 2006, pp. 1–106. doi: 10.1016/B978-0-12-370610-2.50006-4

[11] H. J. Joo and H. Y. Kwak, “Experimental analysis of thermal performance according to heat pipe working fluids for evacuated tube solar collector,” *Heat and Mass Transfer/Waerme- und Stoffuebertragung*, vol. 53, no. 11, pp. 3267–3275, Nov. 2017, doi: 10.1007/s00231-017-2029-0.

[12] W. Rashmi, A. F. Ismail, M. Khalid, and Y. Faridah, “CFD studies on natural convection heat transfer of Al2O 3-water nanofluids,” *Heat and Mass Transfer/Waerme- und Stoffuebertragung*, vol. 47, no. 10, pp. 1301–1310, Oct. 2011, doi: 10.1007/s00231-011-0792-x.

[13] W. Rashmi, M. Khalid, S. S. Ong, and R. Saidur, “Preparation, thermo-physical properties and heat transfer enhancement of nanofluids,” Sep. 01, 2014, *Institute of Physics Publishing*. doi: 10.1088/2053-1591/1/3/032001.

[14] U. SINGH and N. K. GUPTA, “Thermal performance analysis of heat pipe using response surface methdologyUdayvir,” *Journal of Thermal Engineering*, pp. 411–423, Apr. 2023, doi: 10.18186/thermal.1277897.

[15] S. U. S. Choi, J. A. Eastman, and J. A. Eastman, “bTI ENHANCING THERMAL CONDUCTIVITY OF FLUIDS WITH NANOPARTICLES* ENHANCING THERMAL CONDUCTIVITY OF FLUIDS WITH NANOPARTICLES,” 1935.

[16] Mekcem, M.. (2018). Nanofluids and heat pipe limitations. Academic Perspective Procedia, 1 (1), 298-304. DOI: 10.33793/acperpro.01.01.58

[17] S. Kalsi, S. Kumar, A. Kumar, T. Alam, and D. Dobrotă, "Thermophysical properties of nanofluids and their potential applications in heat transfer enhancement: A review," Nov. 01, 2023, *Elsevier B.V.* doi: 10.1016/j.arabjc.2023.105272.

[18] Alkaç, İ.M.; Çerçi, B.; Timuralp, C.; Şen, F. 2—Nanomaterials and their classification. In *Micro and Nano Technologies, Nanomaterials for Direct Alcohol Fuel Cells*; Şen, F., Ed.; Elsevier: Amsterdam, The Netherlands, 2021; pp. 17–33. https://doi.org/10.1016/B978-0-12-821713-9.00011-1

[19] R. Kiran Mudidana, V. Miditana, and V. Rambabu, "Synthesis of nanofluids preparation – A review," *Mater Today Proc*, Sep. 2023, doi: 10.1016/j.matpr.2023.09.086.

[20] W. Safiei, M. M. Rahman, A. R. Yusoff, and M. R. Radin, "Preparation, stability and wettability of nanofluid: A review," *Journal of Mechanical Engineering and Sciences*, vol. 14, no. 3, pp. 7244–7257, Sep. 2020, doi: 10.15282/jmes.14.3.2020.24.0569.

[21] M. Gupta, V. Singh, R. Kumar, and Z. Said, "A review on thermophysical properties of nanofluids and heat transfer applications," 2017, *Elsevier Ltd*. doi: 10.1016/j.rser.2017.02.073.

[22] I. W. Almanassra, A. D. Manasrah, U. A. Al-Mubaiyedh, T. Al-Ansari, Z. O. Malaibari, and M. A. Atieh, "An experimental study on stability and thermal conductivity of water/CNTs nanofluids using different surfactants: A comparison study," *J Mol Liq*, vol. 304, Apr. 2020, doi: 10.1016/j.molliq.2019.111025.

[23] B. Bakthavatchalam, K. Habib, R. Saidur, B. B. Saha, and K. Irshad, "Comprehensive study on nanofluid and ionanofluid for heat transfer enhancement: A review on current and future perspective," May 01, 2020, *Elsevier B.V.* doi: 10.1016/j.molliq.2020.112787.

[24] K. Elsaid *et al.*, "Thermophysical properties of graphene-based nanofluids," *International Journal of Thermofluids*, vol. 10, May 2021, doi: 10.1016/j.ijft.2021.100073.

[25] G. Latini, "Thermophysical properties of fluids: Dynamic viscosity and thermal conductivity," in *Journal of Physics: Conference Series*, Institute of Physics Publishing, Nov. 2017. doi: 10.1088/1742-6596/923/1/012001.

[26] A. Basu, A. Saha, S. Banerjee, P. C. Roy, and B. Kundu, "A Review of Artificial Intelligence Methods in Predicting Thermophysical Properties of Nanofluids for Heat Transfer Applications," Mar. 01, 2024, *Multidisciplinary Digital Publishing Institute (MDPI)*. doi: 10.3390/en17061351.

[27] A. Faghri and Y. Zhang, "Fundamentals of Multiphase Heat Transfer and Flow."

[28] R. S. Vajjha, D. K. Das, and B. M. Mahagaonkar, "Density measurement of different nanofluids and their comparison with theory," *Pet Sci Technol*, vol. 27, no. 6, pp. 612–624, Apr. 2009, doi: 10.1080/10916460701857714.

[29] Einstein, A. (1906), Eine neue Bestimmung der Moleküldimensionen. Ann. Phys., 324: 289-306. https://doi.org/10.1002/andp.19063240204

[30] B. Barbés *et al.*, "Thermal conductivity and specific heat capacity measurements of Al 2O3 nanofluids," *J Therm Anal Calorim*, vol. 111, no. 2, pp. 1615–1625, Feb. 2013, doi: 10.1007/s10973-012-2534-9.

[31] C. Y. Tsai, H. T. Chien, P. P. Ding, B. Chan, T. Y. Luh, and P. H. Chen, "Effect of structural character of gold nanoparticles in nanofluid on heat pipe thermal performance," *Mater Lett*, vol. 58, no. 9, pp. 1461–1465, Mar. 2004, doi: 10.1016/j.matlet.2003.10.009.

[32] G. Kumaresan, S. Venkatachalapathy, and I. C. Naik, "An experimental study on improvement in thermal efficiency of mesh wick heat pipe," in *Applied Mechanics and Materials*, Trans Tech Publications Ltd, 2014, pp. 1423–1427. doi: 10.4028/www.scientific.net/AMM.592-594.1423.

[33] G. Kumaresan, S. Venkatachalapathy, and L. G. Asirvatham, "Experimental investigation on enhancement in thermal characteristics of sintered wick heat pipe using CuO nanofluids," *Int J Heat Mass Transf*, vol. 72, pp. 507–516, May 2014, doi: 10.1016/j.ijheatmasstransfer.2014.01.029.

[34] W. I. A. Aly, M. A. Elbalshouny, H. M. Abd El-Hameed, and M. Fatouh, "Thermal performance evaluation of a helically-micro-grooved heat pipe working with water and aqueous Al2O3 nanofluid at different inclination angle and filling ratio," *Appl Therm Eng*, vol. 110, pp. 1294–1304, Jan. 2017, doi: 10.1016/j.applthermaleng.2016.08.130.

[35] N. S. Pandya, A. N. Desai, A. Kumar Tiwari, and Z. Said, "Influence of the geometrical parameters and particle concentration levels of hybrid nanofluid on the thermal performance of axial grooved heat pipe," *Thermal Science and Engineering Progress*, vol. 21, Mar. 2021, doi: 10.1016/j.tsep.2020.100762.

[36] Wang, X., Wen, Q., Yang, J., Shittu, S., Wang, X., Zhao, X., & Wang, Z. (2023). Heat transfer and flow characteristic of a flat confined loop thermosyphon with ternary hybrid nanofluids for electronic devices cooling. *Applied Thermal Engineering*, *221*. https://doi.org/10.1016/j.applthermaleng.2022.119758

[37] M. M. Sarafraz, F. Hormozi, and S. M. Peyghambarzadeh, "Thermal performance and efficiency of a thermosyphon heat pipe working with a biologically ecofriendly nanofluid," *International Communications in Heat and Mass Transfer*, vol. 57, pp. 297–303, 2014, doi: 10.1016/j.icheatmasstransfer.2014.08.020.

[38] H. Hassan and S. Harmand, "Effect of using nanofluids on the performance of rotating heat pipe," *Appl Math Model*, vol. 39, no. 15, pp. 4445–4462, Aug. 2015, doi: 10.1016/j.apm.2014.12.023.

[39] T. Tharayil, L. G. Asirvatham, V. Ravindran, and S. Wongwises, "Thermal performance of miniature loop heat pipe with graphene-water nanofluid," *Int J Heat Mass Transf*, vol. 93, pp. 957–968, Feb. 2016, doi: 10.1016/j.ijheatmasstransfer.2015.11.011.

[40] M. R. Tanshen, B. Munkhbayar, M. J. Nine, H. Chung, and H. Jeong, "Effect of functionalized MWCNTs/water nanofluids on thermal resistance and pressure fluctuation characteristics in oscillating heat pipe," *International Communications in Heat and Mass Transfer*, vol. 48, pp. 93–98, Nov. 2013, doi: 10.1016/j.icheatmasstransfer.2013.08.011.

[41] K. H. Do and S. P. Jang, "Effect of nanofluids on the thermal performance of a flat micro heat pipe with a rectangular grooved wick," *Int J Heat Mass Transf*, vol. 53, no. 9–10, pp. 2183–2192, Apr. 2010, doi: 10.1016/j.ijheatmasstransfer.2009.12.020.

[42] A. Shirazi, R. A. Taylor, G. L. Morrison, and S. D. White, "Solar-powered absorption chillers: A comprehensive and critical review," Sep. 01, 2018, *Elsevier Ltd*. doi: 10.1016/j.enconman.2018.05.091.

[43] Q. Ma, T. Lan, Y. Lai, X. Luo, and P. He, "Application of the cooling measures in the highway roadbed in permafrost regions of the Qinghai-Tibet Plateau," *Cold Reg Sci Technol*, vol. 221, May 2024, doi: 10.1016/j.coldregions.2024.104177.

[44] S. Du and Z. Ye, “Analysis and Applications of the Two Phases Closed Thermosyphon Technology in the Highways in Permafrost Regions: A Review,” May 01, 2024, *Multidisciplinary Digital Publishing Institute (MDPI)*. doi: 10.3390/app14104185.

[45] A. M. Wagner, “Review of Thermosyphon Applications.” [Online]. Available: https://www.researchgate.net/publication/266672789

[46] K. Rongchai and S. Tundee, “Development, testing and design optimisation of a water and R134a based thermosyphon heat exchanger for air-water heat recovery systems,” *Case Studies in Thermal Engineering*, vol. 39, Nov. 2022, doi: 10.1016/j.csite.2022.102453.

[47] V. Guichet, S. Almahmoud, and H. Jouhara, “Nucleate pool boiling heat transfer in wickless heat pipes (two-phase closed thermosyphons): A critical review of correlations,” Oct. 01, 2019, *Elsevier Ltd*. doi: 10.1016/j.tsep.2019.100384.

[48] N. Y. Londoño Pabón, J. P. Florez Mera, G. Serafin Couto Vieira, and M. Barbosa Henriques Mantelli, “Visualization and experimental analysis of Geyser boiling phenomena in two-phase thermosyphons,” *Int J Heat Mass Transf*, vol. 141, pp. 876–890, Oct. 2019, doi: 10.1016/j.ijheatmasstransfer.2019.06.052.

[49] H. Jouhara, B. Fadhl, and L. C. Wrobel, “Three-dimensional CFD simulation of geyser boiling in a two-phase closed thermosyphon,” *Int J Hydrogen Energy*, vol. 41, no. 37, pp. 16463–16476, 2016, doi: 10.1016/j.ijhydene.2016.02.038.

[50] S. Sichamnan, T. Chompookham, and T. Parametthanuwat, “A case study on internal flow patterns of the two-phase closed thermosyphon (TPCT),” *Case Studies in Thermal Engineering*, vol. 18, Apr. 2020, doi: 10.1016/j.csite.2020.100586.

[51] D. Bhuyan, “Direct and Indirect Contact Filmwise as well as Dropwise Condensation of Water Vapour with and without Noncondensible Gas-A Review,” *International Research Journal of Engineering and Technology*, 2020.

[52] D. Seo, J. Shim, D. H. Shin, Y. Nam, and J. Lee, “Dropwise condensation of acetone and ethanol for a high-performance lubricant-impregnated thermosyphon,” *Int J Heat Mass Transf*, vol. 181, Dec. 2021, doi: 10.1016/j.ijheatmasstransfer.2021.121871.

[53] Y. Gao *et al.*, “Application of nanofluids in heat pipes,” Jun. 01, 2023, *Springer Science and Business Media B.V.* doi: 10.1007/s10973-023-12115-2.

[54] A. Gallego, B. Herrera, R. Buitrago-Sierra, C. Zapata, and K. Cacua, “Influence of filling ratio on the thermal performance and efficiency of a thermosyphon operating with Al2O3-water based nanofluids,” *Nano-Structures and Nano-Objects*, vol. 22, Apr. 2020, doi: 10.1016/j.nanoso.2020.100448.

[55] M. M. Sarafraz, F. Hormozi, and S. M. Peyghambarzadeh, “Thermal performance and efficiency of a thermosyphon heat pipe working with a biologically ecofriendly nanofluid,” *International Communications in Heat and Mass Transfer*, vol. 57, pp. 297–303, 2014, doi: 10.1016/j.icheatmasstransfer.2014.08.020.

[56] M. M. Sarafraz, O. Pourmehran, B. Yang, and M. Arjomandi, “Assessment of the thermal performance of a thermosyphon heat pipe using zirconia-acetone nanofluids,” *Renew Energy*, vol. 136, pp. 884–895, Jun. 2019, doi: 10.1016/j.renene.2019.01.035.

[57] Q. Xu *et al.*, “A comparative investigation on the effect of different nanofluids on the thermal performance of two-phase closed thermosyphon,” *Int J Heat Mass Transf*, vol. 149, Mar. 2020, doi: 10.1016/j.ijheatmasstransfer.2019.119189.

[58] A. Kamyar, K. S. Ong, and R. Saidur, "Effects of nanofluids on heat transfer characteristics of a two-phase closed thermosyphon," *Int J Heat Mass Transf*, vol. 65, pp. 610–618, 2013, doi: 10.1016/j.ijheatmasstransfer.2013.06.046.

[59] L. Asmaie, M. Haghshenasfard, A. Mehrabani-Zeinabad, and M. Nasr Esfahany, "Thermal performance analysis of nanofluids in a thermosyphon heat pipe using CFD modeling," *Heat and Mass Transfer/Waerme- und Stoffuebertragung*, vol. 49, no. 5, pp. 667–678, May 2013, doi: 10.1007/s00231-013-1110-6.

[60] W. W. o *et al.*, "A two-phase closed thermosyphon operated with nanofluids for solar energy collectors: Thermodynamic modeling and entropy generation analysis," *Solar Energy*, vol. 211, pp. 192–209, Nov. 2020, doi: 10.1016/j.solener.2020.09.031.

[61] Z. hua Liu, X. fei Yang, G. san Wang, and G. liang Guo, "Influence of carbon nanotube suspension on the thermal performance of a miniature thermosyphon," *Int J Heat Mass Transf*, vol. 53, no. 9–10, pp. 1914–1920, Apr. 2010, doi: 10.1016/j.ijheatmasstransfer.2009.12.065.

[62] S. Baek *et al.*, "Experimental Study on the Enhanced Thermal Performance of Two-Phase Closed Thermosyphon Using Mechanical and Chemical Treated MWCNTs Nanofluids," *Microgravity Sci Technol*, vol. 33, no. 2, Apr. 2021, doi: 10.1007/s12217-021-09872-w.

[63] S. Zhao, G. Xu, N. Wang, and X. Zhang, "Experimental study on the thermal start-up performance of the graphene/water nanofluid-enhanced solar gravity heat pipe," *Nanomaterials*, vol. 8, no. 2, Feb. 2018, doi: 10.3390/nano8020072.

[64] D. Choi and K. Y. , "Experimental study on confinement effect of two-phase closed thermosyphon and heat transfer enhancement using cellulose nanofluid," *Appl Therm Eng*, vol. 183, Jan. 2021, doi: 10.1016/j.applthermaleng.2020.116247.

[65] D. Choi, G. Jun, W. Hwang, and K. Y. Lee, "Heat transfer enhancement of small-diameter two-phase closed thermosyphon using cellulose nanofiber and hydrophilic surface modification," *Nanomaterials*, vol. 11, no. 3, pp. 1–20, Mar. 2021, doi: 10.3390/nano11030647.

[66] C. hee Lee, S. W. Seo, D. K. Park, and K. Y. Lee, "Influence of cellulose nanofiber fluid on flow instability and heat transfer of two-phase closed thermosyphon," *Heliyon*, vol. 9, no. 10, Oct. 2023, doi: 10.1016/j.heliyon.2023.e20925.

[67] Maxwell, J.C. (1873) A Treatise of Electricity and Magnetism. Clarendon Press, Oxford.

[68] R. L. Hamilton and O. K. Crosser, "Thermal Conductivity of Heterogeneous Two-Component Systems," *Ind. Eng. Chem. Fund.*, vol. 1, no. 3, pp. 187–191, Aug. 1962, doi: 10.1021/i160003a005

[69] S. Goudarzi, M. Shekaramiz, A. Omidvar, E. Golab, A. Karimipour, and A. Karimipour, "Nanoparticles migration due to thermophoresis and Brownian motion and its impact on Ag-MgO/Water hybrid nanofluid natural convection," *Powder Technol*, vol. 375, pp. 493–503, Sep. 2020, doi: 10.1016/j.powtec.2020.07.115.

[70] R. Harish and R. Sivakumar, "Effects of nanoparticle dispersion on turbulent mixed convection ows in cubical enclosure considering Brownian motion and thermophoresis," *Powder Technol*, vol. 378, pp. 303–316, Jan. 2021, doi: 10.1016/j.powtec.2020.09.054.

[71] S. P. Jang and S. U. S. Choi, "Effects of various parameters on nanofluid thermal conductivity," *J Heat Transfer*, vol. 129, no. 5, pp. 617–623, May 2007, doi: 10.1115/1.2712475.

[72] M. Borzuei and Z. Baniamerian, “Role of nanoparticles on critical heat flux in convective boiling of nanofluids: Nanoparticle sedimentation and Brownian motion,” *Int J Heat Mass Transf*, vol. 150, Apr. 2020, doi: 10.1016/j.ijheatmasstransfer.2019.119299.

[73] Y. Li, Y. Zhai, M. Ma, Z. Xuan, and H. Wang, “Using molecular dynamics simulations to investigate the effect of the interfacial nanolayer structure on enhancing the viscosity and thermal conductivity of nanofluids,” *International Communications in Heat and Mass Transfer*, vol. 122, Mar. 2021, doi: 10.1016/j.icheatmasstransfer.2021.105181.

[74] Y. Zhai, Y. Li, Z. Xuan, Z. Li, and H. Wang, “Determination of heat transport mechanism using nanoparticle property and interfacial nanolayer in a nanofluidic system,” *J Mol Liq*, vol. 344, Dec. 2021, doi: 10.1016/j.molliq.2021.117787.

[75] R. Pal, “A novel method to determine the thermal conductivity of interfacial layers surrounding the nanoparticles of a nanofluid,” *Nanomaterials*, vol. 4, no. 4, pp. 844–855, Dec. 2014, doi: 10.3390/nano4040844.

[76] M. M. Sarafraz, I. Tlili, M. A. Baseer, and M. R. Safaei, “Potential of solar collectors for clean thermal energy production in smart cities using nanofluids: Experimental assessment and efficiency improvement,” *Applied Sciences (Switzerland)*, vol. 9, no. 9, May 2019, doi: 10.3390/app9091877.

[77] A. Isogai, “Cellulose Nanofibers: Recent Progress and Future Prospects,” 2020, *Society of Fiber Science and Technology*. doi: 10.2115/FIBERST.2020-0039.

[78] W. K. Hwang, S. Choy, S. L. Song, J. Lee, D. S. Hwang, and K. Y. Lee, “Enhancement of nanofluid stability and critical heat flux in pool boiling with nanocellulose,” *Carbohydr Polym*, vol. 213, pp. 393–402, Jun. 2019, doi: 10.1016/j.carbpol.2019.03.023.

[79] N. Rajendran, T. Runge, R. D. Bergman, P. Nepal, N. Nair, and W. Ashraf, “Economic and environmental impact analysis of cellulose nanofiber-reinforced concrete mixture production,” *Resour Conserv Recycl*, vol. 212, Jan. 2025, doi: 10.1016/j.resconrec.2024.107917.

[80] Y. Zhang *et al.*, “Effect of mesh number of wood powder and ratio of raw materials on properties of composite material of starch/wood powder,” *Bioresources*, vol. 10, no. 3, pp. 5345–5355, 2015, doi: 10.15376/biores.10.3.5345-5355.

[81] D. A. Gkika *et al.*, “Price tag in nanomaterials?,” *Journal of Nanoparticle Research*, vol. 19, no. 5, May 2017, doi: 10.1007/s11051-017-3875-x.

[82] D. Moon, M. Sagisaka, K. Tahara, and K. Tsukahara, “Progress towards sustainable production: Environmental, economic, and social assessments of the cellulose nanofiber production process,” *Sustainability (Switzerland)*, vol. 9, no. 12, Dec. 2017, doi: 10.3390/su9122368.

[83] W. Najahi-Missaoui, R. D. Arnold, and B. S. Cummings, “Safe nanoparticles: Are we there yet?,” *Int J Mol Sci*, vol. 22, no. 1, pp. 1–22, Jan. 2021, doi: 10.3390/ijms22010385.

[84] A. R. I. Ali and B. Salam, “A review on nanofluid: preparation, stability, thermophysical properties, heat transfer characteristics and application,” Oct. 01, 2020, *Springer Nature*. doi: 10.1007/s42452-020-03427-1.

[85] M. Mekcem, M. Berkani, and M. Bilgili, “IMPACT OF FILLING RATIO AND CELLULOSE NANOFIBER NANOFLUID ON THE TOTAL THERMAL RESISTANCE AND THE STARTUP OF A MINIATURE THERMOSYPHON,” 2024. Volume 55, Issue 17, 2024, pp. 1-12. DOI: 10.1615/HeatTransRes.2024051883

[86] Yunus A.Cengel. Heat and Mass Transfer. 3rd edition. Chapter7: External forced convection. McGraw-Hill, New York, 2007.

[87] Holman, J. P. (n.d.). Experimental Methods for Engineers. Seventh Edition. McGraw-Hill, Singapore, 2001

[88] A. Ozsoy and V. Corumlu, "Thermal performance of a thermosyphon heat pipe evacuated tube solar collector using silver-water nanofluid for commercial applications," *Renew Energy*, vol. 122, pp. 26–34, Jul. 2018, doi: 10.1016/j.renene.2018.01.031.

[89] X. Wang, Y. Wang, H. Chen, and Y. Zhu, "A combined CFD/visualization investigation of heat transfer behaviors during geyser boiling in two-phase closed thermosyphon," *Int J Heat Mass Transf*, vol. 121, pp. 703–714, Jun. 2018, doi: 10.1016/j.ijheatmasstransfer.2018.01.005.

[90] M. Ghanbarpour, N. Nikkam, R. Khodabandeh, and M. S. Toprak, "Improvement of heat transfer characteristics of cylindrical heat pipe by using SiC nanofluids," *Appl Therm Eng*, vol. 90, pp. 127–135, Jul. 2015, doi: 10.1016/j.applthermaleng.2015.07.004.

[91] T. Grab, U. Gross, U. Franzke, and M. H. Buschmann, "Operation performance of thermosyphons employing titania and gold nanofluids," *International Journal of Thermal Sciences*, vol. 86, pp. 352–364, 2014, doi: 10.1016/j.ijthermalsci.2014.06.019.

[92] M. H. Buschmann and U. Franzke, "Improvement of thermosyphon performance by employing nanofluid," *International Journal of Refrigeration*, vol. 40, pp. 416–428, 2014, doi: 10.1016/j.ijrefrig.2013.11.022.

[93] S. Lee, R. A. Taylor, L. Dai, R. Prasher, and P. E. Phelan, "The effective latent heat of aqueous nanofluids," *Mater Res Express*, vol. 2, no. 6, Jun. 2015, doi: 10.1088/2053-1591/2/6/065004.

[94] B. Fadhl, L. C. Wrobel, and H. Jouhara, "Numerical modelling of the temperature distribution in a two-phase closed thermosyphon," *Appl Therm Eng*, vol. 60, no. 1–2, pp. 122–131, 2013, doi: 10.1016/j.applthermaleng.2013.06.044.

[95] T. Zhang, L. Wang, W. Zheng, Z. Yan, and J. Hou, "Parametric analysis on flooding limit and critical film thickness of a vertical two-phase closed thermosyphon," *Heat and Mass Transfer/Waerme- und Stoffuebertragung*, vol. 57, no. 1, pp. 1–12, Jan. 2021, doi: 10.1007/s00231-020-02941-7.

[96] V. Guichet and H. Jouhara, "Condensation, evaporation and boiling of falling films in wickless heat pipes (two-phase closed thermosyphons): A critical review of correlations," Feb. 01, 2020, *Elsevier B.V.* doi: 10.1016/j.ijft.2019.100001.

[97] P. Estellé, D. Cabaleiro, G. Żyła, L. Lugo, and S. M. S. Murshed, "Current trends in surface tension and wetting behavior of nanofluids," Oct. 01, 2018, *Elsevier Ltd*. doi: 10.1016/j.rser.2018.07.006.

[98] A. Kujawska, R. Mulka, M. H. Buschmann, Z. Krolicki, and B. Zajaczkowski, "Impact of Silica Nanofluid Deposition on Thermosyphon Performance," *Heat Transfer Engineering*, vol. 42, no. 19–20, pp. 1702–1719, 2021, doi: 10.1080/01457632.2020.1818413.

[99] X. Ma, Z. Zhao, P. Jiang, S. Yang, S. Li, and X. Chen, "Investigation of start-up characteristics of thermosyphons modified with different hydrophilic and hydrophobic inner surfaces," *Energies (Basel)*, vol. 13, no. 3, 2020, doi: 10.3390/en13030765.

[100] S. Suresh, K. P. Venkitaraj, P. Selvakumar, and M. Chandrasekar, "Synthesis of Al2O3-Cu/water hybrid nanofluids using two step method and its thermo physical properties," *Colloids Surf A*

Physicochem Eng Asp, vol. 388, no. 1–3, pp. 41–48, Sep. 2011, doi: 10.1016/j.colsurfa.2011.08.005.

[101] A. Ahmadi Nadooshan, H. Eshgarf, and M. Afrand, "Measuring the viscosity of Fe3O4-MWCNTs/EG hybrid nanofluid for evaluation of thermal efficiency: Newtonian and non-Newtonian behavior," *J Mol Liq*, vol. 253, pp. 169–177, Mar. 2018, doi: 10.1016/j.molliq.2018.01.012.

[102] W. Yu, H. Xie, L. Chen, and Y. Li, "Investigation of thermal conductivity and viscosity of ethylene glycol based ZnO nanofluid," *Thermochim Acta*, vol. 491, no. 1–2, pp. 92–96, Jul. 2009, doi: 10.1016/j.tca.2009.03.007.

[103] M. Klazly and G. Bognár, "A novel empirical equation for the effective viscosity of nanofluids based on theoretical and empirical results," *International Communications in Heat and Mass Transfer*, vol. 135, Jun. 2022, doi: 10.1016/j.icheatmasstransfer.2022.106054.

Appendices

Appendix.1

Find more information at **nanografi.com** Contact us at **sales@nanografi.com**

nanografi

NANOGRAFI NANOTECHNOLOGY

TECHNICAL DATA SHEET

PRODUCT INFORMATION

Product Group	Nanoparticles
Trade Name	Cellulose Nanofiber (Cellulose Nanofibril, Nanofibrillated Cellulose, CNFs)
Modified Cellulose FiberCAS#:	68442-85-3
Natural Cellulose FiberCAS#:	65996-61-4
Water CAS#:	7732-18-5
Product Number	NG01NC0201

PRODUCT PROPERTIES

Cellulose Nanocrystal

Appearance (Color)	White
Appearance (Form)	Dry powder (~4 wt.% moisture)
Average Particle Size	10-20 nm wide, 2-3 µm length
Cellulose Crystallinity (XRD)	92%
Decomposition Temperature (TGA in N2)	329 °C
Density	1.50 g/cm3

CERTIFICATE OF ANALYSIS

Test Items	Specification	Test Results
Appearence		Yellow powder
Odor		None
Content	wt (%) (110 °C, 5h)	99.6 %
Ash	<15 % (880 °C,2 hours)	12.3 %

Appendix.1

NANOGRAFI NANOTECHNOLOGY

Ion conductivity	<2000 us/cm (1 wt% solution)	824.0 us/cm
PH	6-8 (1wt% solution)	7.0
Maximum particle Size	<1 um /1 cm filter)	conform
-OH content	>2.0 mmol/g	2.51 mmol/g

APPLICATION

Cellulose Nano fibril is originally generated from wood-derived fibrils with length in the micrometer and width in the nanometric range during the biosynthesis of cellulose.

Today, there is widespread scientific and commercial interest in cellulose nano fibrils (CNF). There have several application areas including foods, cosmetics, pharmaceuticals, paints, drilling muds, paper additives and paperboard barriers, medical products, etc. Our Nano fibrillated Cellulose product competes on price and performance with counterparts.

Appendix .1

Find more information at **nanografi.com** Contact us at **sales@nanografi.com**

NANOGRAFI NANOTECHNOLOGY

TEM IMAGE OF PRODUCT

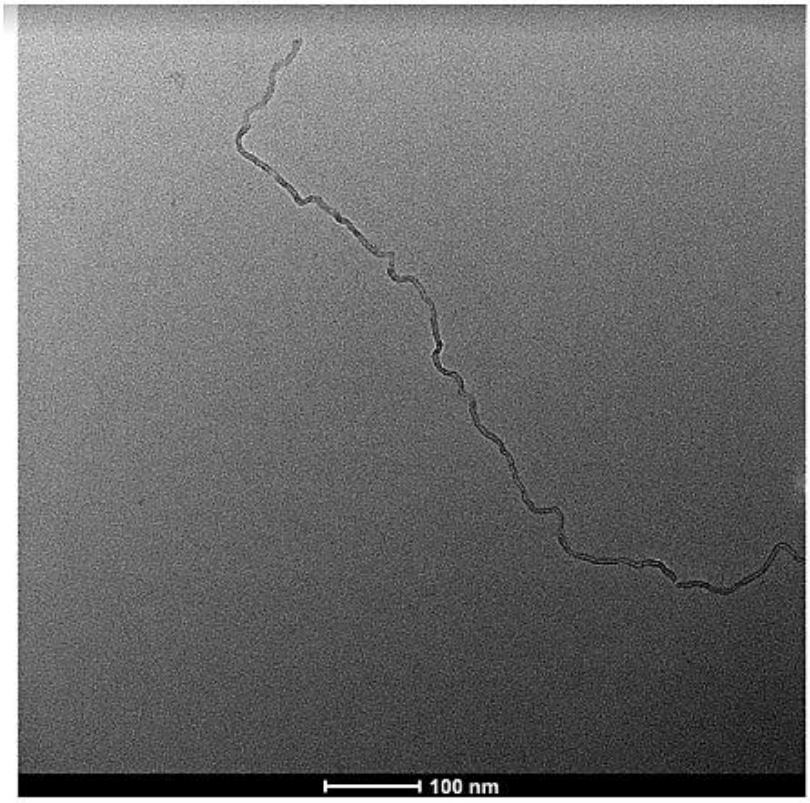

Appendix .2

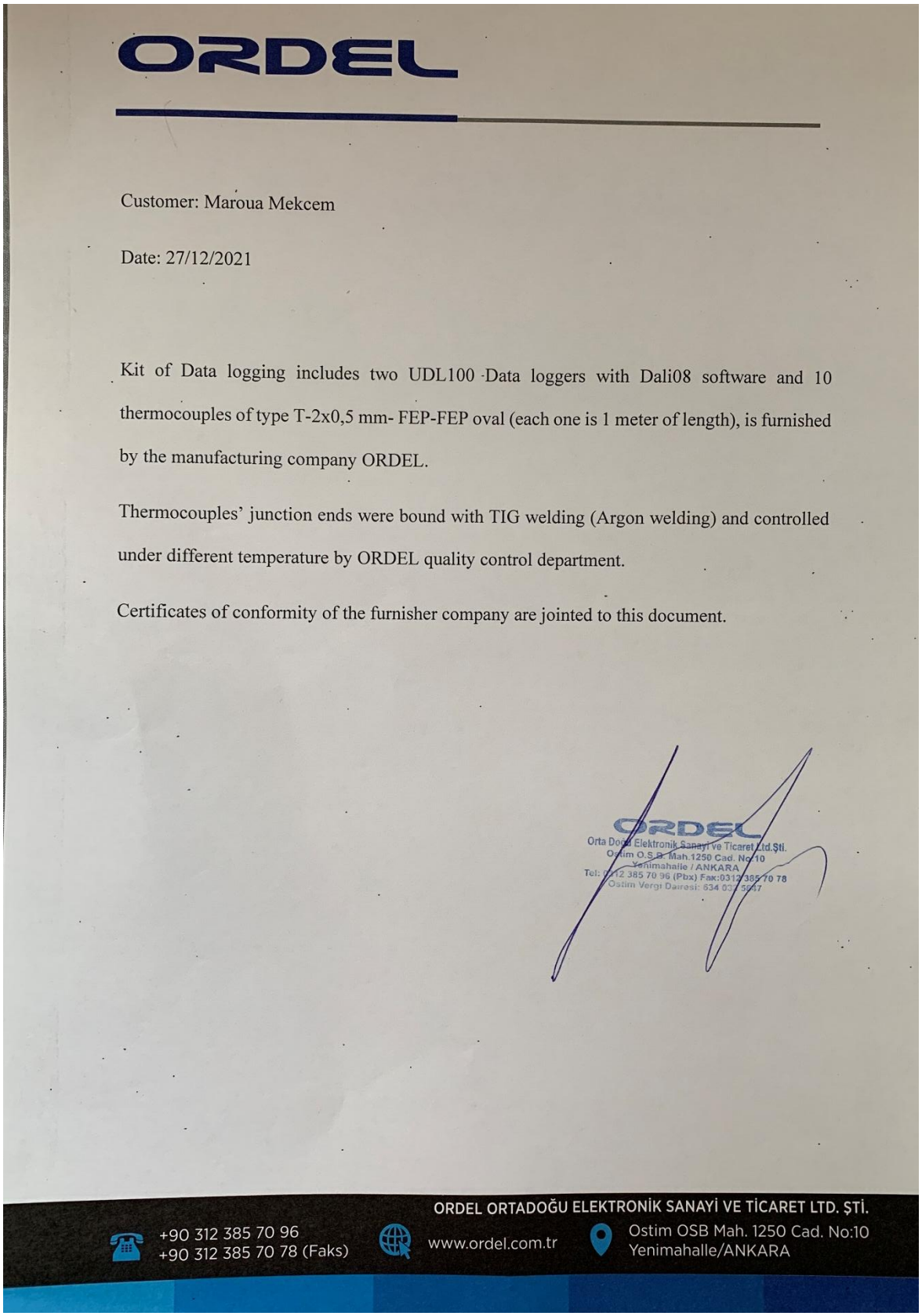

ORDEL

Customer: Maroua Mekcem

Date: 27/12/2021

Kit of Data logging includes two UDL100 Data loggers with Dali08 software and 10 thermocouples of type T-2x0,5 mm- FEP-FEP oval (each one is 1 meter of length), is furnished by the manufacturing company ORDEL.

Thermocouples' junction ends were bound with TIG welding (Argon welding) and controlled under different temperature by ORDEL quality control department.

Certificates of conformity of the furnisher company are jointed to this document.

ORDEL
Orta Doğu Elektronik Sanayi Ve Ticaret Ltd.Şti.
Ostim O.S.B. Mah.1250 Cad. No:10
Yenimahalle / ANKARA
Tel: 0312 385 70 96 (Pbx) Fax:0312 385 70 78
Ostim Vergi Dairesi: 634 027 5067

ORDEL ORTADOĞU ELEKTRONİK SANAYİ VE TİCARET LTD. ŞTİ.
+90 312 385 70 96
+90 312 385 70 78 (Faks)
www.ordel.com.tr
Ostim OSB Mah. 1250 Cad. No:10
Yenimahalle/ANKARA